Predicting Subsidence Resulting from Tunnel Excavation

by

George Thai

A thesis
presented to the University of Waterloo
in fulfillment of the
thesis requirement for the degree of
Master of Applied Science
in
Civil Engineering

Waterloo, Ontario, Canada, 2010

Author's Declaration

I hereby declare that I am the sole author of this thesis. This is a true copy of the thesis, including any required final revisions, as accepted by my examiners. I understand that my thesis may be made electronically available to the public.

Abstract

As a result of tunnel construction, the ground level surface above will tend to collapse downward as the soil seeks to refill the missing tubular cavity. Many infrastructures that were originally built on that surface may also fall slightly or severely depending on the engineering design and execution of the tunneling project. Engineers then must factor in the development of ground subsidence, examining geotechnical and geological issues to construct a model that would otherwise predict the extent of vertical settlements. Their predictions could help to assess potential damages and make corrective actions. In this thesis submission, analytical methods from the classical elasticity were used to estimate surface displacements for a prospective tunnel.

The analytical equation tied in the method of virtual images originating from Sagaseta with the classical Kirsch elastic solutions for stress-displacements of an infinite plate with hole in order to establish a solution of half-space. This approach will be similar to what Verruijt-Booker had developed after Sagaseta but will include higher-order terms to simulate an excavation process in a longitudinal direction below ground and thereby obtain a new subsidence equation including ground parameters associated with tunnel shape changes occurring at its base, springline (sideway point) and crown (top). These parameters were not previously reported by the Verruijt-Booker work or from current technical literature. In addition, the prescribed solution could include any Poisson' ratios in which only the original Verruijt-Booker could be found correct for only incompressibility conditions ($\upsilon = 0.5$). The Verruijt-Booker equation considered deep tunnels only. An extra term influencing the subsidence was included in the modified solution which is significant for shallow tunnels.

The derived equations were applied to calculate surface deflections using data from a tunnel construction project to test its viability. Comparison analysis was made with the three methods to be described- Peck, Sagaseta, and Verruijt-Booker. In addition, a parametric study was made to examine the amount of subsidence changed when deciding to construct a tunnel from a shallow to deeper zone. Finally, a qualitative study of the derived equation and Verruijt-Booker was conducted to assess potential subsidence behaviour between shallow and deep tunnels.

Acknowledgement

I wish to express my gratitude to Dr. L. Rothenburg for giving me the opportunity to investigate this research topic on tunnel induced ground subsidence for the completion of my thesis requirement. I am gratified of him for sharing his expertise and patience during my development of this research. The important insight I obtained out of this research was seeing that the theory of elasticity remains ever relevant today as was developed many years ago for various applications. This specialized displacement analysis induced by tunneling action was my exposure and contribution in this branch of engineering mechanics. Finally, special thanks for their constructive reviews by Dr. G. Cascante and Dr. L. S. Matott to improve this thesis.

Dedication

There are two groups of people who I would like to express my dedication. First, my parents who did not endow me any technical training but brought me here anyways to find out for myself what research is all about. Secondly, to the engineering and applied mechanics community at large who bring complex mathematics down from the level of abstraction to one of practicality.

Table of Contents

List of Figures

Chapter 1 Introduction

A recurring problem in municipal or major urban center is the planning of transportation systems needed to bring its citizenry from various points to another. One important component of this solution is the construction of public transit networks that co-mingles with other private vehicle users but nevertheless delivers the people to their intended destination with minimal delays in a large urban traffic system. In addition to the benefits of easing congestion, there is an environmental impact when the emissions of pollutants from waiting automobiles are released during daily stops.

While not being the total solution of environmental and traffic problems, the engineering design and construction of railway tunnels below ground has been one of the favorable option city planners look to. One can think of London (UK), Washington D.C, New York City, Paris, and Tokyo are such prime examples as densely populated centers having to deliberately construct tunnel networks for subway trains connecting to certain important nodes or points decided by governmental and consulting firms.

The engineering of tunnel construction must be examined at multiple viewpoints to ensure the safety of the surroundings is maintained. A typical tunneling project would consist of a detailed geological and geotechnical analysis, routing issues, data monitoring programs, and preliminary to final approval of the tunnel design itself. An important component recognized by engineers that is integrated in that project is the prospect that foundations of buildings may settle due to the boring activities. Depending on the tunnel diameter and depth below, the volume excavated will force the soil to immediately or in due course cover up the opening gap. Even if

reinforced liners are installed around the circumference, there will still be soil movement that will envelop the liners and potentially leave significant depression space for the foundation to move downwards.

There are current numerical and analytical studies conducted to monitor subsidence as the tunnel boring machines (TBM) advances [2, 5, 8, 15, 17, 18, 20, 21]. The analytical work relies on the theory of elasticity [27, 29]. Of the many prominent researchers, Peck [22] was one of the originators who suggested that the vertical settlements matched the patterns of the Gaussian or normal distribution curve. Later on, closed form solutions were proposed independently first by Sagaseta [23], and years after generalized by Verruijt and Booker [29]. Sagaseta suggested that strain field is based on an isotropic and homogeneous incompressibility of the soil caused by near-surface ground loss. He was the original developer of the concept of virtual images in formulating displacements, a concept that was subsequently refined by others. The Verruijt-Booker method extended the solution of Sagaseta in terms of ground loss, not necessarily for the incompressible condition, applicable to any Poisson ratio values and included the effects of ovalization of the tunnel opening.

Tunnel subsidence can be measured with varying accuracy with either empirical or computational means. In studies using the empirical approach, a gap parameter has been extensively investigated by Lee, Rowe et al [13, 14] to measure the ground loss. Using finite element analysis data and traditional geotechnical engineering, the researchers were able to construct N-Ω graphs, and develop calculation guidelines for quantifying the physical gap, elastoplastic deformation and workmanship at the tunnel face. These three components are to be added together to obtain a numerical gap value. In general, ground loss measures the material volume that has been removed in excess of the theoretical design volume of excavation. This

particular quantity provides a field-based indicator to possibly calibrate with analytical modeling work.

An alternative method for predicting subsidence considers elasticity theory. More directly, the contribution of this utilized the Kirsch solution of a hole in an infinite plate and combine those results with the virtual image technique introduced nearly a century later by Sagaseta. The approach here adopts a procedure somewhat similar to Verruijt and Booker but takes on a general analysis which includes higher-order terms appearing in the elastic equations. The outcome of this approach is the derivation of coefficients which measure the distortion and radial strain of an excavated tunnel, as well as development of general displacement equations for both horizontal and vertical directions. In particular, a subsidence or vertical surface displacement equation was obtained to estimate soil movement downwards when disturbed by the bored tunnel. In addition, by normalizing some aspects of the subsidence equation, some inferences may be made to predict responses of the settlements.

The organization of the remaining thesis is summarized as follows. Chapter 2 further describes the causes of subsidence and how to measure it in actual construction. A brief introduction of the Peck method is discussed due to its ubiquitous application at many sites. Chapter 3 and 4 provides the analytical background and tools required to establish the displacement equations. In Chapter 5, numerical results and qualitative observations are made. Finally, Chapter 6 provides the conclusions that summarize the entire findings and contributions.

Chapter 2 Description of Subsidence Problem

2.1 Introduction

The problem of determining vertical displacement or subsidence of the ground level due to subsurface tunneling is an important endeavor as engineers must be aware of adjacent and existing structures on top may collapse as the foundation soil seeks to cover up the excavated opening. Essentially, the tunnel boring machines (TBM) shown in Figure 2.1 advances forward through a prescribed design route creating a cylindrical cavity or tube. The resulting cavity would then cause the surrounding soil to move towards it and immediately fill up so as to restore to its original state of equilibrium. This caving in phenomenon is unavoidable irrespective of the geographic location and type of non-uniform geological layers for tunnel construction projects around the world [24].

As depicted in Figure 2.2, the gap between the original ground surface and deflection produces unwanted slopes that would otherwise force the foundations of facilities to slide along and destabilize the structure causing severe damages. Engineers must then develop some geomechanical model that will predict the extent of these displacements in order to recommend and plan reinforcement options that will minimize potential foundation collapse. While the focus of this tunneling subsidence modeling is in the domain of civil engineering, it could also be extended towards mining and petroleum engineering operations since they involve tubular underground excavation to obtain useful natural resources [24][30].

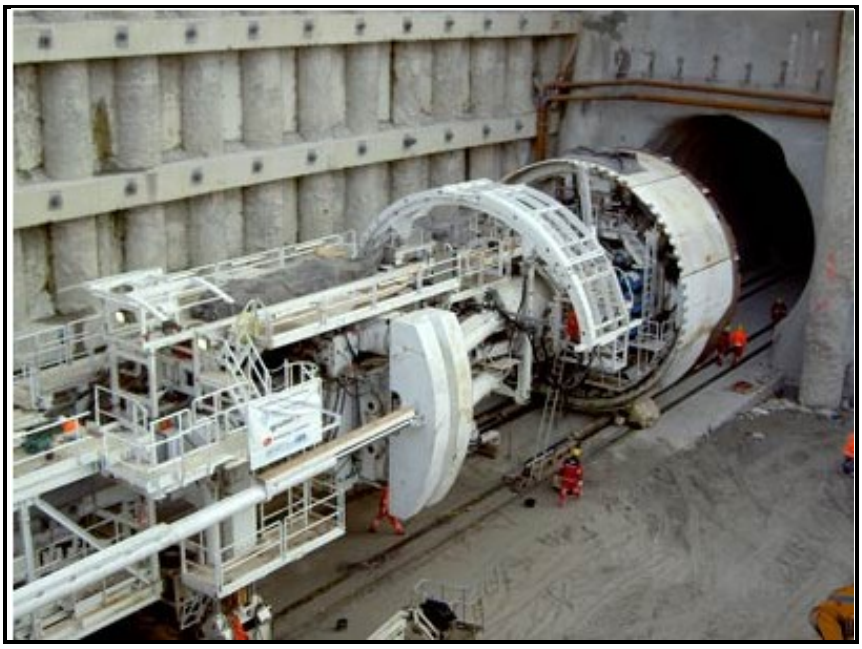

Fig.2.1 Tunnel boring machine (TBM) used to excavate cylindrical opening [AlpTransit Gotthard Ltd. http://www.alptransit.ch/pages/e/].

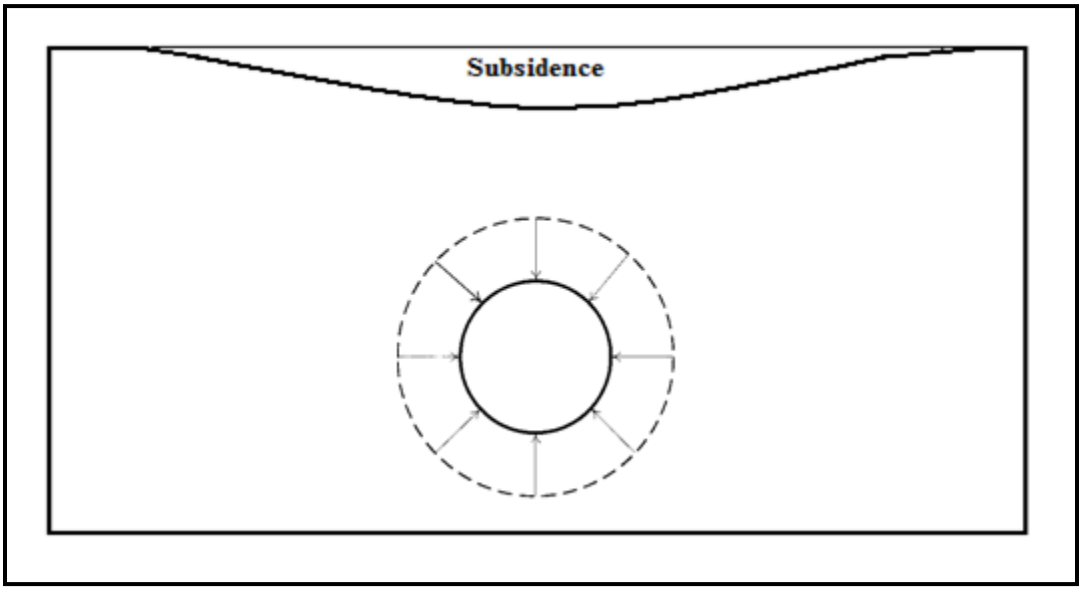

Fig.2.2 Tunneling activities represented by the circle will cause the surrounding soil to collapse indicated by the arrows. Engineers must determine the amount of subsidence to prevent any nearby or overlying structures from falling in.

2.2 Subsidence Causes

Subsidence may be described by the ground loss attributed by the excavation of soil from the surface below. In the context of tunnel engineering, the result of the tunnel boring machine (TBM) creating an underground opening allows the surrounding soil to become mobile so as to fill in the cavity. This soil movement towards covering the excavated void is known as the ground or volume loss, which in turn measures the amount of subsidence, or surface deflections that would be induced by subsurface boring operations.

In numerical modeling of ground losses, the aim is to account for certain factors encountered during the construction stage so as to obtain a reliable prediction of settlements. These factors depend on data collected from soil properties, machine operations and previous case histories. All this information forms a quantitative measure called the gap parameter (g) which gauges the ground loss at the tunnel crown. In order to compute g, engineers using prior tunneling cases have formulated a systematic procedure requiring key measurements to be made as the TBM progresses from a distanced segment to the next. These measurements must be made at three stages that occur simultaneously: (1) front or face (2) on top of the shield and (3) the rear of the TBM where the linings are installed. Furthermore, the path traversed by the TBM may encounter varying alignments and this influences the calculation of g. Displacements measured at these three positions of the TBM are then used to compute g.

The gap parameter consisted of adding some or all three components together depending on the traversed alignment [13, 14]. The general case may be stated as

$$g = G_p + u^*_{3D} + \omega \tag{2.2.1}$$

where g is the gap parameter, G_p is the physical gap between the vertical distance of the tunnel lining crown and shield, u_{3D}^* is referred as a spatial elastic-plastic deformation which factors in potential three dimensional movements in front of the tunnel path and ω defined as a workmanship factor due to steering issues. Since g is a length measure, the units for each component that are added up can be expressed in millimeters (mm). The significance of each term will be discussed below and for proper use of Eq. (2.2.1) depends upon recognizing on the constructional alignment.

The alignment path can be generally categorized into three distinct construction procedural cases as shown in Figure 2.3. In case (i), g is exactly equal to G_p because the TBM face is in full contact at the soil with minor stress and strain changes at the frontal contact interface leaving negligible horizontal gaps. In addition, the advancing path of the TBM shield is essentially flat without any deviations. The actual value (g=G_p) is then taken at the lining platform or behind the shield. For case (ii), potential longitudinal displacements in front of the TBM face are included in g $\left(g = G_p + u_{3D}^*\right)$but the traversed pathway remains fairly leveled. It should be noted that the spatial deformation term could be simplified by using a planar approximation. Finally, all possible difficulties encountered during the boring operations can be factored in by extending case (ii) to include a workmanship factor ω. Thus case (iii) has incorporated any effects of extraordinary maneuvers, irregular alignments, and soil reinforcements conforming to the general form defined by Eq. (2.2.1).

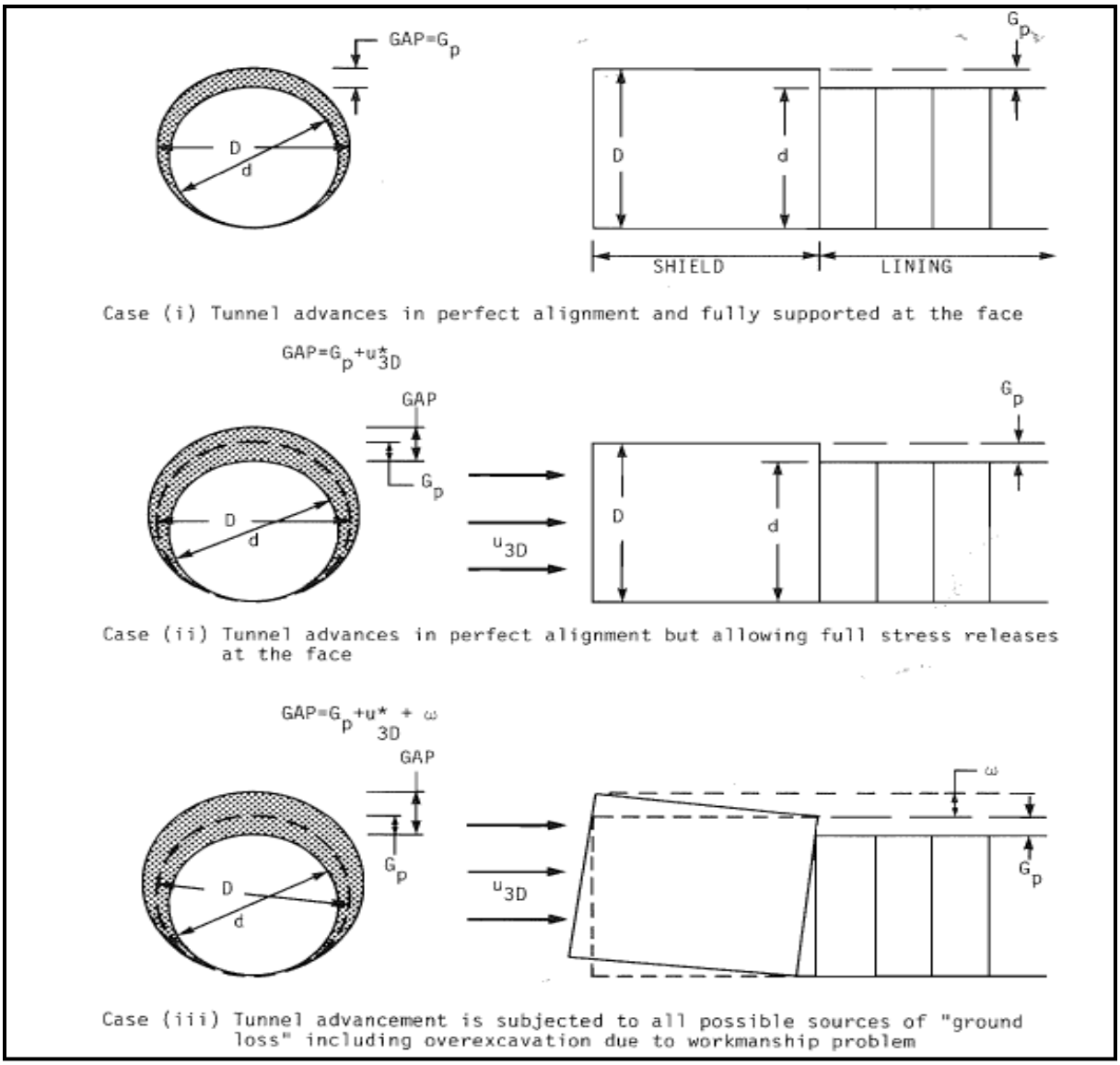

Fig.2.3 Gap parameter usage depending on how the construction progresses [12].

The quantitative evaluation of each of the three terms forming the gap parameter will now be examined. The individual terms were established by Lee et al. and have specific calculation rules regarding the usage of TBM shield and lining dimensions, soil parameters and charts.

2.3 Peck's Method

The empirical method of Peck is often quoted in current tunnel engineering literature [8, 12, 17, 18]. Its simplicity is that the pattern of the subsidence can be idealized as a normal distribution reflected downwards to resemble the deflections induced by tunnel excavation below ground. The equation states the vertical deflection u_z can be expressed as

$$u_z = u_{\max} \exp\left(-\frac{x^2}{2i^2}\right) \tag{2.3.1}$$

where u_{max} is the maximum settlement over the tunnel axis, x is the distance to the tunnel centerline and i is the inflection point in the normal distribution curve as shown in Figure 2.4. The inflection point is also equal to the standard deviation of the normal probability curve and could be interpreted as the magnitude of the settlement trough width. Often, the determination of i is related to the soil property and depth of the tunnel to be obtained during construction [17].

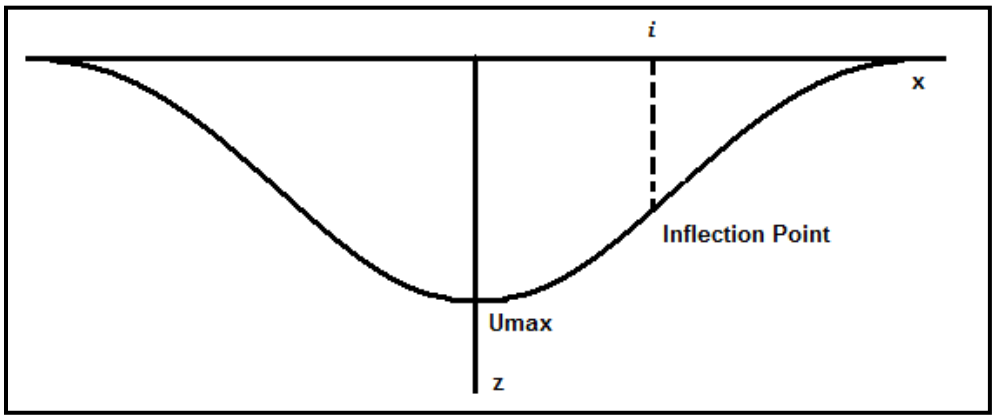

Fig.2.4 The reflected normal curve approximates the settlement trough due to tunneling according to Peck.

The volume loss (V_s) can be defined as the removed volume per meter run of excavated area and is equivalent to integrating (2.3.1). The integration process takes advantage of the special modified Gaussian integral [26]

$$\int_{-\infty}^{\infty} \exp\left(-ax^2\right)dx = \sqrt{\frac{\pi}{a}},\ a > 0 \tag{2.3.2}$$

Now substituting $a = \frac{1}{2i^2}$ into (2.3.2) establishes

$$V_s = u_{\max}\int_{-\infty}^{\infty} \exp\left(-\frac{x^2}{2i^2}\right)dx = iu_{\max}\sqrt{2\pi} \tag{2.3.3}$$

With (2.3.3), u_{max} can be solved to get $u_{\max} = \frac{V_s}{i\sqrt{2\pi}} = \frac{V_s}{2.5i}$, and then re-inserted into (2.3.1) to obtain the Peck deflection equation at the surface $u_{z[0]}$

$$u_{z[0]} = \frac{V_s}{2.5i}\exp\left(-\frac{x^2}{2i^2}\right) \tag{2.3.4}$$

As suggested by Peck, the parameter *i* could be approximated by a normalized diagram he devised as shown in Figure 2.5 below,

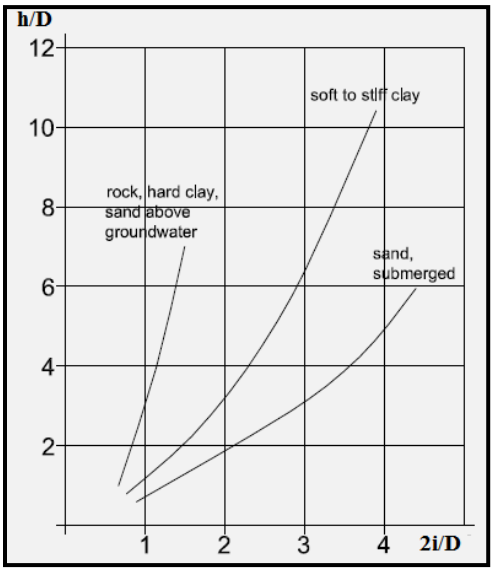

Fig.2.5 Determining inflection point based on normalized parameters [9].

or according to the following Clough-Schmidt [3, 9] empirical formula

$$i = \left(\frac{D}{2}\right)\left(\frac{h}{D}\right)^{4/5} \tag{2.3.5}$$

where h denotes the depth of the tunnel axis, and D is the diameter of the cavity opening. The potential range of values to estimate i as suggested in Figure 2.5 could belong into various soil characteristics. Other modifications of Eq. (2.3.5) are suggested in recent investigations, but the principal objective is remains to find i if the method of Peck is to be used.

There are several caveats of using (2.3.4) including that it over-predicts the surface displacement when compared to other methods including analytical and field measurements. Another deficiency is that it cannot include any soil property parameter into the equation for displacement estimations. In addition, the Peck equation is only applicable to one particular layer, that is the ground level, and leaves out intermediated gaps for analyzing subsurface strata if need be. Finally, there is no corresponding lateral ground movement formulation that can be investigated using this method.

2.4 Plane Strain Analysis

A plane strain analysis was assumed for the analytical model work. At the outset, the hypothetical tunnel can be assumed to be a cylindrical prismatic body and have lateral loads applied uniformly along an axis outside the xz-plane (Figure 2.6). This assumption does not allow any displacement and strains along the y-direction of the tunnel. Thus, any deformation of the ground can be also assumed to be independent of the y-coordinate [1, 23]. Since conditions are similar at all cross sections, only a slice between two sections can be studied making a two dimensional analysis possible.

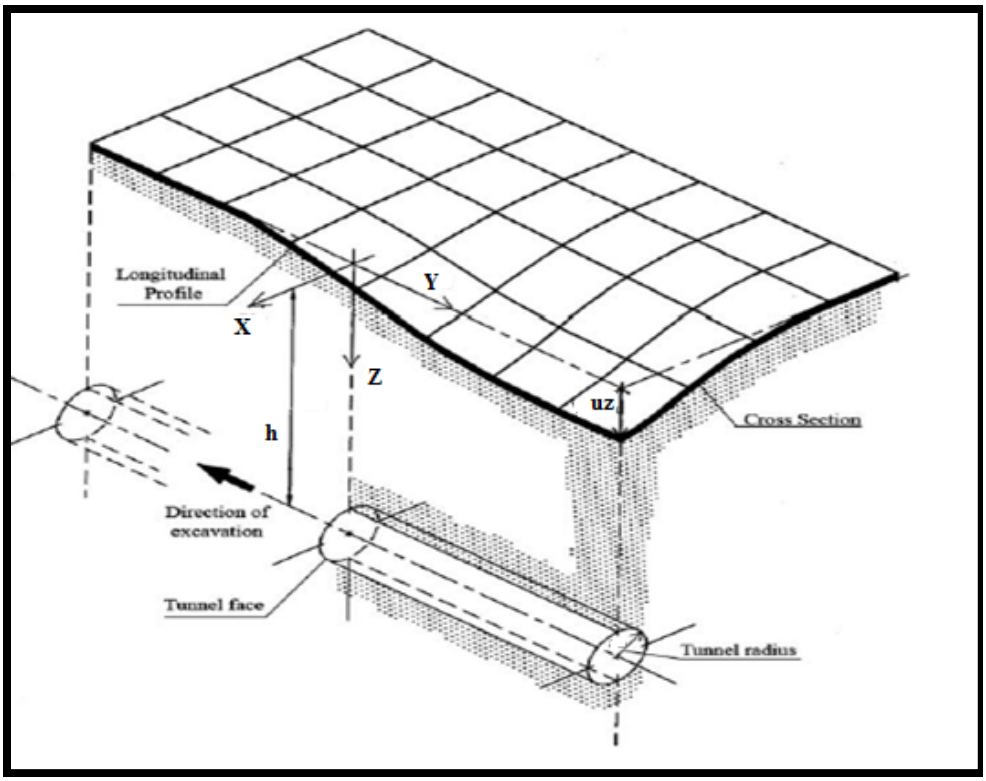

Fig.2.6 Plane strain assumption for tunnel induced subsidence model. The length of the tunnel is larger than the dimensions of the circular opening [18].

Chapter 3 Tunnel Deformations

3.1 Closed-form Solutions for Tunnel Deformations

The objective of determining the subsidence equation is to predict a certain amount of ground level deflections dependent on the tunnel deformation geometry as shown in Figure 3.1 below. The total deformation considers the total contribution from the ground loss and ovalization [5]. As will be discussed later on, the ground loss is also equivalent to an evaluation for radial strain which may be considered a summed average of the total crown (top) and springline (side) of the cavity; likewise, the ovalization a differenced average between the crown and springline.

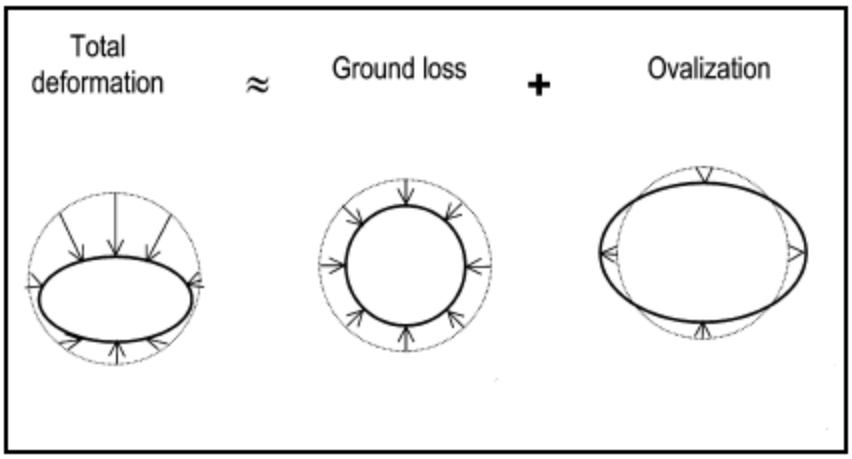

Fig.3.1 Subsidence model incorporates the combined effects of ground loss and ovalization [5].

Closed- form solutions for tunnel deformations have been developed using various mathematical methods. As will be described below, Sagaseta presented a procedure of converting a half-space to full space problem and used concepts from fluid mechanics to develop the displacement equations. In addition, a brief discussion of the Verruijt-Booker (VB) equation will be described with respect to influence of a radial strain and ovalization parameter along with some problems associated with its use. The two parameters in the VB equation parallel the two

components on the right-side of the diagram in Figure 3.1. The corrections for the VB will be provided in the next chapter which incorporates higher-order terms.

3.2 Sagaseta's Method

The principal concepts behind the Sagaseta method is the so-called virtual image procedure and comprised of some features modeled from fluid mechanics but modified for use in geomechanics [23]. This modification directly replaces the velocities as a quantity from fluid flow into displacements. In a real physical situation, there are no normal and shear stresses present at the ground surface. The use of a virtual image in the full-space would eliminate the stress acting on the free ground surface

In brief, the analysis considers that a stress applied below (sink) a plane of symmetry has a dual image across that plane, essentially doubling the stress amount which in turn allows displacements to be determined. Any influence of the free surface could then be incorporated at the end of the solution. The method also assumes the soil medium to be infinite, and be homogeneously isotropic.

The Sagaseta method as depicted in Figure 3.2 consists of three main steps and is applicable with respect to shallow tunnel analysis.

(1) A point sink in an infinite medium should be used to calculate strains ignoring any soil surface effects.

(2) The strains computed in (1) will cause surface level stresses and must be counterbalanced by determining these stresses. Two sub-methods may be considered:

i. Using a virtual source, a projected negative (or positive) mirror image of the actual sink reflecting from the top surface can act as an opposite normal and shear stresses.

ii. Add the image-based strains (or stresses) to those found in step (1).

(3) Obtain a displacement field in a half-space influenced by the load on the surface equal and opposite from the calculated portion of step (2). This result is added to the displacements found in step (1).

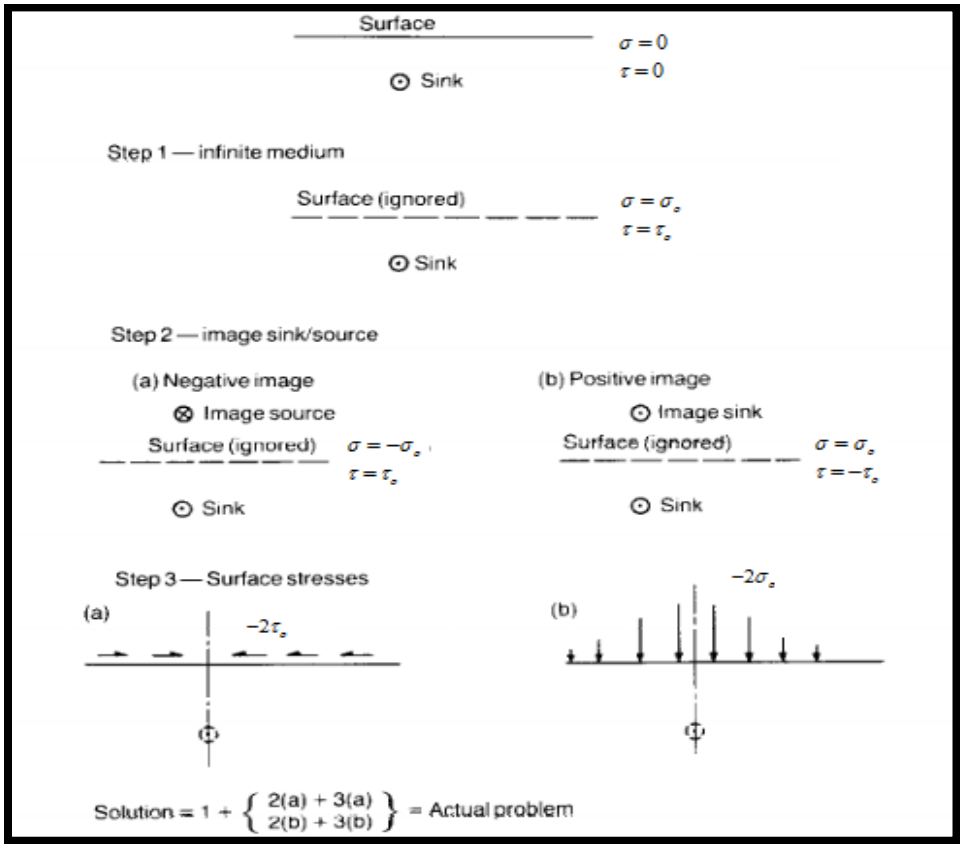

Fig.3.2 Sagaseta procedure outlining the use of the virtual image in order to develop a final displacement solution. A half-space problem becomes a full-space in this method [21].

As discussed from incompressible potential flow theory concerning sinks and sources, there is no angular velocity but only a radial component [7]. A point sink may then be represented as

$$v_r = \frac{Q}{2\pi r} \quad \Leftrightarrow \quad U = \frac{\varepsilon R^2}{2r} \tag{3.2.1}$$

where v_r is called the radial velocity. In the fluid-to-geomechanics analogy, Q (flow rate) is equivalent to the volume loss and when substituted derives the radial displacement U. Here, U was simply replaced for v_r. For a two dimensional analysis, the horizontal (u_x) and vertical (u_z) displacements from the sink to an arbitrary point located below the ground surface were obtained by using

$$u_x = U\cos\theta \tag{3.2.2}$$

$$u_z = U\sin\theta \tag{3.2.3}$$

or in analytic form

$$u_x = -\frac{\varepsilon R^2}{2}\frac{x - x_o}{r^2} \tag{3.2.4}$$

$$u_z = -\frac{\varepsilon R^2}{2}\frac{z - z_o}{r^2} \tag{3.2.5}$$

where $r^2 = (x - x_o)^2 + (z - z_o)^2$.

By step 2, the displacements represented by the sink part is added to the negative image resulting

$$u_x = -\frac{\varepsilon R^2}{2}\left(\frac{x}{r_1^2} - \frac{x}{r_2^2}\right) \tag{3.2.6}$$

and

$$u_z = -\frac{\varepsilon R^2}{2}\left(\frac{z_1}{r_1^2} - \frac{z_2}{r_2^2}\right) \tag{3.2.7}$$

where

$$\left.\begin{aligned} z_1 &= z - h \\ z_2 &= z + h \\ r_1^2 &= x^2 + z_1^2 \\ r_2^2 &= x^2 + z_2^2 \end{aligned}\right\} \tag{3.2.8}$$

and h may be considered the tunnel placement depth measured from the opening centre to ground surface. With respect to subsidence at the ground level, variable z is set to zero into (3.2.6) and (3.2.7) yielding

$$u_x = -\frac{2\varepsilon R^2 x}{x^2 + h^2} \tag{3.2.9}$$

$$u_z = \frac{2\varepsilon R^2 h}{x^2 + h^2} \tag{3.2.10}$$

An alternative form of the lateral and vertical deflections may be considered if a quantity called the volume loss (V_s) is defined as

$$V_s = 2\varepsilon\pi R^2 \tag{3.2.11}$$

Then, by inserting (3.2.11) into Eqs. (3.2.9) and (3.2.10) establishes

$$u_x = -\frac{V_s x}{\pi\left(x^2 + h^2\right)} \tag{3.2.12}$$

$$u_z = \frac{V_s h}{\pi\left(x^2 + h^2\right)} \tag{3.2.13}$$

3.3 Verruijt-Booker's Method

The Verruijt-Booker (VB) equations [29] were originally stated without providing details towards its development as

$$\begin{aligned} u_x = -\varepsilon R^2 x\left(\frac{1}{r_1^2} + \frac{1}{r_2^2}\right) + \delta R^2 x\left(\frac{x^2 - kz_1^2}{r_1^4} + \frac{x^2 - kz_2^2}{r_2^4}\right) \\ - \frac{2\varepsilon R^2}{n}\left(\frac{1}{r_2^2} - \frac{2nzz_2}{r_2^4}\right) - \frac{4\delta R^2 hx}{n+1}\left[\frac{z_2}{r_2^4} + \frac{nz\left(x^2 - 3z_2^2\right)}{r_2^6}\right] \end{aligned} \tag{3.3.1}$$

$$u_z = -\varepsilon R^2 x\left(\frac{z_1}{r_1^2}+\frac{z_2}{r_2^2}\right)+\delta R^2\left[z_1\left(\frac{kx^2-z_1^2}{r_1^4}\right)+z_2\left(\frac{kx^2-z_2^2}{r_2^4}\right)\right]$$
$$+2\varepsilon R^2\left(\frac{1+n}{n}\right)\left(\frac{z_2}{r^2}\right)-2\varepsilon R^2 z\left(\frac{x^2-z_2^2}{r_2^4}\right) \qquad (3.3.2)$$
$$-\frac{2\delta R^2 h}{r_2^4}\left(x^2-z_2^2\right)-\frac{2\delta R^2 hzn}{n+1}\left[\frac{2z_2}{r_2^6}\left(3x^2-z_2^2\right)\right]$$

with $k=\frac{\upsilon}{1-\upsilon}$. For the special case at the ground level z = 0, the subsidence becomes

$$u_z = 2\varepsilon R^2\left(\frac{1+n}{n}\right)\left(\frac{h}{x^2+h^2}\right)-2\delta R^2 h\frac{x^2-h^2}{\left(x^2+h^2\right)^2} \qquad (3.3.3)$$

or equivalently,

$$u_z = 4\varepsilon R^2\left(1-\upsilon\right)\left(\frac{h}{x^2+h^2}\right)-2\delta R^2 h\frac{x^2-h^2}{\left(x^2+h^2\right)^2} \qquad (3.3.4)$$

where $n=\frac{1}{1-2\upsilon}$ was used.

The essential features of the VB equations are that it was the first to combine the virtual-image method of Sagaseta and equations from the theory of elasticity. Another appealing attribute is that there are two equations to describe both lateral and vertical directions of displacements. In addition, two geotechnical coefficients were introduced which they called ε for the radial strain and δ for the distortion or ovalization of the tunnel thereby include field measurements in order to obtain more refined surface settlement evaluation. Unfortunately, the

formulas for these terms were never explicitly defined so as to compute their values in the original derivation. This deficiency will be addressed in the next chapter including the entire development of a general solution that will treat the VB equations as a special case.

The VB equation can better describe tunnels that are placed at farther depths below ground. The influencing variable in this case is the Poisson's ratio υ at 0.5. A heave should be experienced close to the tunnel centerline at the surface but according to the VB model, this should occur when $x>h$. In addition the VB solution asserts that the shape of the settlement profile while independent of υ, tends to increase if υ decreases from 0.5 to 0. These two attributes are contradictory to the general expressions developed in Chapter 4 and discussed in Chapter 5.

Chapter 4 Higher-Order Derivation

4.1 Generalized Verruijt-Booker Method

The approach adopted here for the development of the Verruijt-Booker solutions will be connected to the elasticity problem of determining the biaxial stresses applied onto a central cylindrical opening in an infinite plate. The originators of these elastic equations did not explicitly mention their procedure for their derivation, but in this thesis ideas from elasticity, solid mechanics, linear algebra and operational methods will attempt to generalize their solution. In the presentation to follow, linear terms used represented a solid soil matrix without any removed hole and higher order terms were retained to model an excavated hole. The final horizontal and vertical displacement shall be demonstrated to have the form

$$u_x = u_{x[1]} + u_{x[2]} \tag{4.1.1}$$

$$u_z = u_{z[1]} + u_{z[2]} \tag{4.1.2}$$

where the bracket subscript notation denotes the real $x[1]$ or $z[1]$ and $x[2]$ or $z[2]$ are the virtual image-based displacements. In addition, the subsidence equation was shown to contain two similar parameters and re-stated in normalized form to make qualitative observations presented in Chapter 5.

In this problem, the Airy stress function could be used to satisfy the compatibility equations denoted by the bi-harmonic operator. Using certain boundary conditions, a stress solution could be obtained and in turn displacement equations may be derived. These special stress solutions are referred to as the Kirsch equations and maybe applied to tunnel subsidence models.

In order to proceed, some basic elasticity relationships are reviewed and the problem of a plate without a hole subjected to uniaxial stresses is considered. Based on the problem analogy, the next step extends to the plate with a hole but made use of its prior analysis to build on the solution leading to the equations of Kirsch.

In polar coordinates, the bi-harmonic equation is specified as

$$\nabla^4\Phi = \left(\frac{\partial^2}{\partial r^2} + \frac{1}{r}\frac{\partial}{\partial r} + \frac{1}{r^2}\frac{\partial^2}{\partial \theta^2}\right)\left(\frac{\partial^2\Phi}{\partial r^2} + \frac{1}{r}\frac{\partial\Phi}{\partial r} + \frac{1}{r^2}\frac{\partial^2\Phi}{\partial \theta^2}\right) = 0 \tag{4.1.3}$$

and the corresponding polar Airy stress function Φ defined as

$$\sigma_r = \frac{1}{r}\frac{\partial\Phi}{\partial r} + \frac{1}{r^2}\frac{\partial^2\Phi}{\partial\theta^2} \tag{4.1.4}$$

$$\sigma_\theta = \frac{1}{r^2}\frac{\partial^2\Phi}{\partial r^2} \tag{4.1.5}$$

$$\tau_{r\theta} = -\frac{\partial}{\partial r}\left(\frac{1}{r}\frac{\partial\Phi}{\partial r}\right) \tag{4.1.6}$$

In various elasticity treatises, the infinite plate without hole problem and with stress applied uniaxially, as depicted in Figure 4.1, considers the trial solution Φ to have the rectangular form as

$$\Phi = \frac{py^2}{2} \tag{4.1.7}$$

where p denotes horizontal stress actions. By conversion into polar coordinates, Eq. (4.1.7) becomes

$$\Phi = \frac{pr^2}{4}(1-\cos 2\theta) \tag{4.1.8}$$

Applying the stress equation defined by Eqs. (4.1.4), (4.1.5), and (4.1.6) obtains

$$\sigma_r = \frac{p}{2}(1+\cos 2\theta) \tag{4.1.9}$$

$$\sigma_\theta = \frac{p}{2}(1-\cos 2\theta) \tag{4.1.10}$$

$$\tau_{r\theta} = -\frac{p}{2}\sin 2\theta \tag{4.1.11}$$

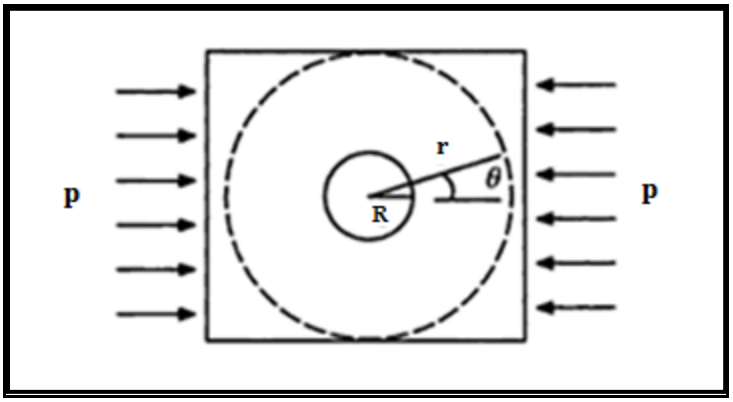

Fig.4.1 Plate subjected to constant stress applied in the horizontal direction [31].

In extending the analogy with that of an inserted circular opening, the Φ function will be assumed to comprise the form

$$\Phi = \phi_1(r) + \phi_2(r)\cos 2\theta \tag{4.1.12}$$

and when substituted as individual components $\phi_1(r)$ and $\phi_2(r)\cos 2\theta$ into Eq. (4.1.3) a pair ordinary differential equation are obtained as

$$\left(\frac{d^2}{dr^2}+\frac{1}{r}\frac{d}{dr}\right)\left(\frac{d^2\phi_1}{dr^2}+\frac{1}{r}\frac{d\phi_1}{dr}\right)=0 \tag{4.1.13}$$

$$\left(\frac{d^2}{dr^2}+\frac{1}{r}\frac{d}{dr}-\frac{4}{r^2}\right)\left(\frac{d^2\phi_2}{dr^2}+\frac{1}{r}\frac{d\phi_2}{dr}-\frac{4\phi_2}{r^2}\right)=0 \tag{4.1.14}$$

The first differential equation can be resolved by first expanding it

$$0=\frac{d^4\phi_1}{dr^4}+\frac{d^2}{dr^2}\left(\frac{1}{r}\frac{d\phi_1}{dr}\right)+\frac{1}{r}\frac{d}{dr}\left(\frac{d^2\phi_1}{dr^2}\right)+\frac{1}{r}\frac{d}{dr}\left(\frac{1}{r}\frac{d\phi_1}{dr}\right)$$

$$=\frac{d^4\phi_1}{dr^4}+\frac{1}{r}\frac{d^3\phi_1}{dr^3}+\frac{2}{r^3}\frac{d\phi_1}{dr}-\frac{1}{r^2}\frac{d^2\phi_1}{dr^2}-\frac{1}{r^2}\frac{d^2\phi_1}{dr^2}+\frac{1}{r}\frac{d^3\phi_1}{dr^3}-\frac{1}{r^3}\frac{d\phi_1}{dr}+\frac{1}{r^2}\frac{d^2\phi_1}{dr^2}$$

$$=\frac{d^4\phi_1}{dr^4}+\frac{2}{r}\frac{d^3\phi_1}{dr^3}-\frac{1}{r^2}\frac{d^2\phi_1}{dr^2}+\frac{1}{r^3}\frac{d\phi_1}{dr} \tag{4.1.15}$$

The solution has the form $\phi=e^{mt}$ or by letting $r=e^t$, then $\phi=r^m$. Subsequently, the corresponding characteristic equation is

$$0=m(m-1)(m-2)(m-3)+2m(m-1)(m-2)-m(m-1)+m$$

$$=m^4-4m^3+4m^2$$

with roots 0, 0, 2, and 2.

The second differential equation is resolved in a similar manner and yields

$$0 = \frac{d^4\phi_2}{dr^4} + \frac{d^2}{dr^2}\left(\frac{1}{r}\frac{d\phi_2}{dr}\right) - 4\frac{d^2}{dr^2}\left(\frac{\phi_2}{r^2}\right) + \frac{1}{r}\frac{d}{dr}\left(\frac{d^2\phi_2}{dr^2}\right) + \frac{1}{r}\frac{d}{dr}\left(\frac{1}{r}\frac{d\phi_2}{dr}\right)$$
$$- \frac{4}{r}\frac{d}{dr}\left(\frac{\phi_2}{r^2}\right) - \frac{4}{r^2}\frac{d^2\phi_2}{dr^2} - \frac{4}{r^3}\frac{d\phi_2}{dr} + \frac{16\phi_2}{r^4}$$

$$= \frac{d^4\phi_2}{dr^4} + \frac{2}{r}\frac{d^3\phi_2}{dr^3} - \frac{1}{r^2}\frac{d^2\phi_2}{dr^2} + \frac{1}{r^3}\frac{d\phi_2}{dr} - \frac{4}{r^2}\frac{d^2\phi_2}{dr^2} + \frac{8}{r^3}\frac{d\phi_2}{dr} + \frac{8}{r^3}\frac{d\phi_2}{dr} - \frac{24\phi_2}{r^4}$$
$$- \frac{4}{r^3}\frac{d\phi_2}{dr} + \frac{8\phi_2}{r^4} - \frac{4}{r^2}\frac{d^2\phi_2}{dr^2} - \frac{4}{r^3}\frac{d^2\phi_2}{dr^2} + \frac{16\phi_2}{r^4}$$

$$= \frac{d^4\phi_2}{dr^4} + \frac{2}{r}\frac{d^3\phi_2}{dr^3} - \frac{9}{r^2}\frac{d^2\phi_2}{dr^2} + \frac{9}{r^3}\frac{d\phi_2}{dr} \tag{4.1.16}$$

with its characteristic equation designated as

$$0 = m(m-1)(m-2)(m-3) + 2m(m-1)(m-2) - 9m(m-1) + 9m$$

$$= m^4 - 4m^3 - 4m^2 + 16m$$

and respective roots of -2, 0, 2 and 4.

Based on these determined roots, the general solution could be represented as

$$\phi_1(r) = A + B\ln r + Cr^2 + Dr^2 \ln r \tag{4.1.17}$$

$$\phi_2(r) = \frac{E}{r^2} + F + Gr^2 + Hr^4 \tag{4.1.18}$$

Equations (4.1.17) and (4.1.18) are then back-substituted into (4.1.12) and applying the polar stress relations gets

$$\Phi = A + B\ln r + Cr^2 + Dr^2 \ln r + \left(\frac{E}{r^2} + F + Gr^2 + Hr^4\right)\cos 2\theta \tag{4.1.19}$$

$$\sigma_r = \frac{B}{r^2} + 2C + D\left(1 + 2\ln r\right) - \left(\frac{6E}{r^4} + \frac{4F}{r^2} + 2G\right)\cos 2\theta \tag{4.1.20}$$

$$\sigma_\theta = -\frac{B}{r^2} + 2C + D\left(3 + 2\ln r\right) - \left(\frac{6E}{r^4} + 2G + 12Hr^2\right)\cos 2\theta \tag{4.1.21}$$

$$\tau_{r\theta} = \left(-\frac{6E}{r^4} - \frac{2F}{r^2} + 2G + 6Hr^2\right)\sin 2\theta \tag{4.1.22}$$

The seven constants *B, C, D, E, F, G* and *H* may be evaluated by considering firstly, that as *r* converges toward infinity, the stress becomes a finite value σ and so constants *D* and *H* are zero. With *D* and *H* removed, the remaining three equations should be equated with the alike terms to Eqs. (4.1.9), (4.1.10) and (4.1.11) to yield the coefficients

$$p = 4C \tag{4.1.23}$$

$$p = -4G \tag{4.1.24}$$

Finally, consider *r* at the tunnel radius *R*, then σ_r and $\tau_{r\theta}$ becomes zero setting up the following system of equations

$$0 = \frac{B}{R^2} + 2C \tag{4.1.25}$$

$$0 = \frac{6E}{R^4} + \frac{4F}{R^2} + 2G \tag{4.1.26}$$

$$0 = -\frac{6E}{R^4} - \frac{2F}{R^2} + 2G \tag{4.1.27}$$

and then yielding the solutions of $B=-\frac{pR^2}{2}$, $E=-\frac{pR^4}{4}$ and $F=\frac{pR^2}{2}$. Now back-substitute all the lettered constants into (4.1.20), (4.1.21) and (4.1.22) obtains the Kirsch elastic solutions

$$\sigma_r=\frac{p}{2}\left(1-\frac{R^2}{r^2}\right)+\frac{p}{2}\left(1+\frac{3R^4}{r^4}-\frac{4R^2}{r^2}\right)\cos 2\theta \tag{4.1.28}$$

$$\sigma_\theta=\frac{p}{2}\left(1+\frac{R^2}{r^2}\right)-\frac{p}{2}\left(1+\frac{3R^4}{r^4}\right)\cos 2\theta \tag{4.1.29}$$

$$\tau_{r\theta}=-\frac{p}{2}\left(1-\frac{3R^4}{r^4}+\frac{2R^2}{r^2}\right)\sin 2\theta \tag{4.1.30}$$

The preceding described only the horizontal stress actions on the edge of the plate but through similar steps, the solutions are equal to the effects of vertical applications. Once the vertical component analysis has been obtained, then by superposition, the stresses are represented as

$$\sigma_r=\frac{p+q}{2}\left(1-\frac{R^2}{r^2}\right)+\frac{p-q}{2}\left(1+\frac{3R^4}{r^4}-\frac{4R^2}{r^2}\right)\cos 2\theta \tag{4.1.31}$$

$$\sigma_\theta=\frac{p+q}{2}\left(1+\frac{R^2}{r^2}\right)-\frac{p-q}{2}\left(1+\frac{3R^4}{r^4}\right)\cos 2\theta \tag{4.1.32}$$

$$\tau_{r\theta}=-\frac{p-q}{2}\left(1-\frac{3R^4}{r^4}+\frac{2R^2}{r^2}\right)\sin 2\theta \tag{4.1.33}$$

where q denotes the uniaxial applied stress in the vertical direction. This biaxial stress action may be viewed in Figure 4.2 below.

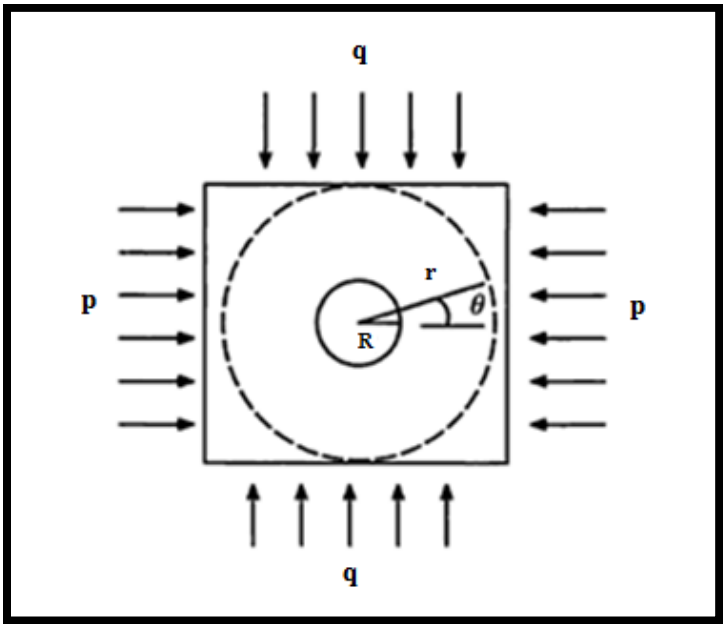

Fig.4.2 Plate subjected by simultaneous horizontal and vertical stresses [31].

The plane strain displacements around the circular opening are then obtained by integrating the respective strain relations defined below.

$$U = \int \varepsilon_r dr = \frac{1}{E}\int (\sigma_r - \upsilon\sigma_\theta) dr = \int \frac{\partial U}{\partial r} dr \tag{4.1.34}$$

$$V = \int (\varepsilon_\theta r - u) d\theta = \int \frac{\partial V}{\partial \theta} d\theta \tag{4.1.35}$$

In the polar system U is referred to as the radial displacement and V called the tangential displacement as shown in Figure 4.3.

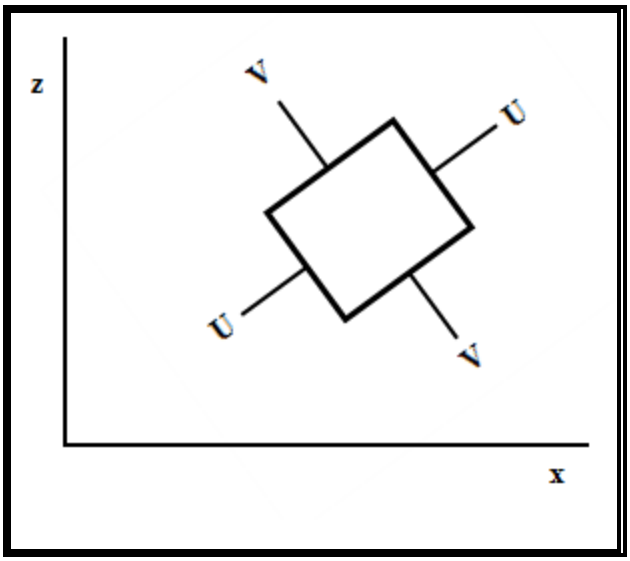

Fig.4.3 Radial and tangential displacement for an element.

It should also be noted that the planar stress solutions may be changed into a planar strain setting based on the material coefficient transformations given as

$$\left.\begin{array}{l} \text{Plane Stress } E \leftrightarrow \dfrac{E}{1-\upsilon^2} \text{ Plane Strain} \\ \text{Plane Stress } \upsilon \leftrightarrow \dfrac{\upsilon}{1-\upsilon} \text{ Plane Strain} \end{array}\right\} \tag{4.1.36}$$

Based on σ_r and σ_θ as defined by (4.1.31) and (4.1.32), the radial and tangential derivatives for (4.1.34) and (4.1.35) are

$$\begin{aligned} \frac{\partial U}{\partial r} = \frac{1}{E}\left[\sigma_a\left(1-\frac{R^2}{r^2}\right)+\sigma_b\left(1-\frac{4R^2}{r^2}+\frac{3R^4}{r^4}\right)\cos 2\theta\right] \\ -\frac{\upsilon}{E}\left[\sigma_a\left(1+\frac{R^2}{r^2}\right)-\sigma_b\left(1+\frac{3R^4}{r^4}\right)\cos 2\theta\right] \end{aligned} \tag{4.1.37}$$

$$\frac{\partial V}{\partial \theta} = -\frac{\sigma_b}{E}\left(2r + \frac{4R^2}{r} + \frac{2R^4}{r^3}\right)\cos 2\theta - \frac{\upsilon\sigma_b}{E}\left(2r - \frac{4R^2}{r} + \frac{2R^4}{r^3}\right)\cos 2\theta \tag{4.1.38}$$

Carrying out the integration of (4.1.37) and (4.1.38) then establishes the results of

$$\begin{aligned} U = \frac{1}{E}\left[\sigma_a\left(r + \frac{R^2}{r}\right) + \sigma_b\left(r - \frac{R^4}{r^3} + \frac{4R^2}{r}\right)\cos 2\theta\right] \\ -\frac{\upsilon}{E}\left[\sigma_a\left(r - \frac{R^2}{r}\right) - \sigma_b\left(r - \frac{R^4}{r^3}\right)\cos 2\theta\right] \end{aligned} \tag{4.1.39}$$

$$V = -\frac{1}{E}\left[\sigma_b\left(r + \frac{2R^2}{r} + \frac{R^4}{r^3}\right)\sin 2\theta\right] - \frac{\upsilon}{E}\left[\sigma_b\left(r - \frac{2R^2}{r} + \frac{R^4}{r^3}\right)\sin 2\theta\right] \tag{4.1.40}$$

and for the planar strain displacement mode, the material coefficients are replaced by transformation Eq. (4.1.36) resulting in

$$\begin{aligned} U = \frac{1-\upsilon^2}{E}\left[\sigma_a\left(r + \frac{R^2}{r}\right) + \sigma_b\left(r - \frac{R^4}{r^3} + \frac{4R^2}{r}\right)\cos 2\theta\right] \\ -\frac{\upsilon(1+\upsilon)}{E}\left[\sigma_a\left(r - \frac{R^2}{r}\right) - \sigma_b\left(r - \frac{R^4}{r^3}\right)\cos 2\theta\right] \end{aligned} \tag{4.1.41}$$

$$V = -\frac{1-\upsilon^2}{E}\left[\sigma_b\left(r + \frac{2R^2}{r} + \frac{R^4}{r^3}\right)\sin 2\theta\right] - \frac{\upsilon(1+\upsilon)}{E}\left[\sigma_b\left(r - \frac{2R^2}{r} + \frac{R^4}{r^3}\right)\sin 2\theta\right] \tag{4.1.42}$$

where σ_a and σ_b are defined by

$$\sigma_a = \frac{p+q}{2} \tag{4.1.43}$$

$$\sigma_b = \frac{p-q}{2} \tag{4.1.44}$$

At this point, the results of (4.1.41) and (4.1.42) will be expanded so as to accommodate the sign convention due to physical interpretation and to incorporate only higher order terms. These special alterations are for the purpose of subsidence modeling. The physical modeling can be viewed in Figure 4.4. On the left side, the plate has not been punctured and only when a hole has been removed, compressive stresses begin to develop around the opening moving outwardly. Consequently, the complete displacement analysis begins with the subtraction of the pre-bored to the excavated cavity thereby establishes a negative sign with respect to the radial and tangential displacements. The higher order terms will represent an excavation and any displacements will be influenced by these terms. Expanding using these assumptions obtains

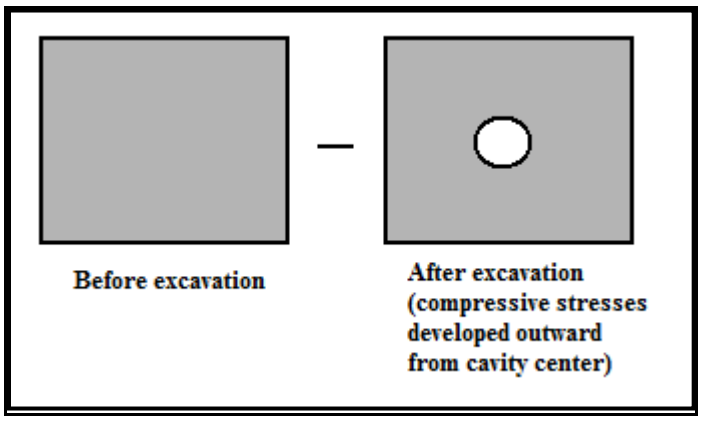

Fig.4.4 Sign convention established by setting the pre-bored medium with that of the excavated.

The higher order terms will represent an excavation and any displacements will be influenced by these terms. Expanding using these assumptions obtains

$$U = -\frac{1-\upsilon^2}{E}\left[\sigma_a \frac{R^2}{r} + \sigma_b\left(\frac{4R^2}{r} - \frac{R^4}{r^3}\right)\cos 2\theta\right] + \frac{\upsilon(1+\upsilon)}{E}\left[-\sigma_a \frac{R^2}{r} + \sigma_b \frac{R^4}{r^3}\cos 2\theta\right]$$

$$= -\frac{(1+\upsilon)}{E}\frac{\sigma_a R^2}{r} - \left(\frac{1-\upsilon^2}{E}\right)\frac{4\sigma_b R^2}{r}\cos 2\theta + \frac{(1+\upsilon)}{E}\frac{\sigma_b R^4}{r^3}\cos 2\theta \tag{4.1.45}$$

$$V = \frac{1-\upsilon^2}{E}\left[\sigma_b\left(\frac{2R^2}{r} + \frac{R^4}{r^3}\right)\sin 2\theta\right] + \frac{\upsilon(1+\upsilon)}{E}\left[\sigma_b\left(\frac{R^4}{r^3} - \frac{2R^2}{r}\right)\sin 2\theta\right]$$

$$= \frac{(1+\upsilon)(1-2\upsilon)}{E}\frac{\sigma_b R^2}{r}\sin 2\theta + \frac{(1+\upsilon)}{E}\frac{\sigma_b R^4}{r^3}\sin 2\theta \tag{4.1.46}$$

The result of interest is when r becomes the tunnel radius R at the wall for the radial component. When substituted into (4.1.45) gets

$$U(r=R) = -\frac{(1+\upsilon)}{E}\sigma_a R - \frac{4(1-\upsilon)(1+\upsilon)}{E}\sigma_b R\cos 2\theta + \frac{(1+\upsilon)}{E}\sigma_b R\cos 2\theta$$

$$= -(1+\upsilon)\frac{\sigma_a R}{E} - \frac{(3-4\upsilon)(1+\upsilon)\sigma_b R}{E}\cos 2\theta \tag{4.1.47}$$

The extreme points with respect to the radial displacement U around the circle may now be examined to determine a set of component-wise vertical and horizontal displacements, and in turn re-write σ_a and σ_b as a special coefficient pair. These points are depicted in Figure 4.5.

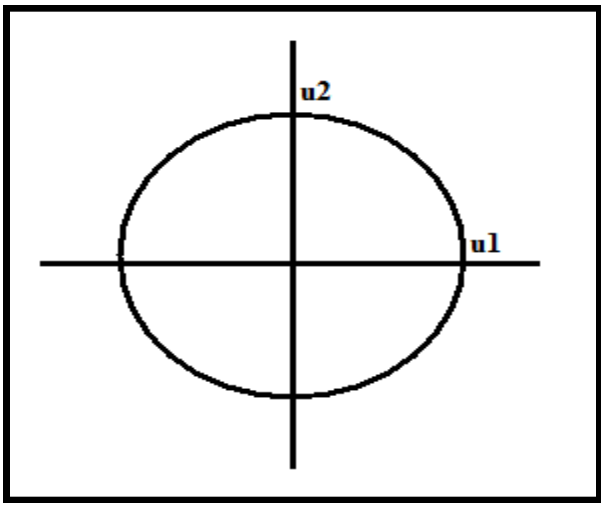

Fig.4.5 Tunnel points of interest for radial displacement.

Taking $\theta = 0$ (for U_1) and $\theta = \frac{\pi}{2}$ (for U_2) as the extreme points in (4.1.47) gets

$$U_1 = -(1+\upsilon)\frac{\sigma_a R}{E} - \frac{(3-4\upsilon)(1+\upsilon)\sigma_b R}{E} \tag{4.1.48}$$

$$U_2 = -(1+\upsilon)\frac{\sigma_a R}{E} + \frac{(3-4\upsilon)(1+\upsilon)\sigma_b R}{E} \tag{4.1.49}$$

Adding (4.1.48) and (4.1.49) leads to

$$\sigma_a = \frac{\varepsilon E}{1+\upsilon} \tag{4.1.50}$$

where ε is a dimensionless coefficient defined by

$$\varepsilon = -\frac{U_1 + U_2}{2R} \tag{4.1.51}$$

Similarly, the difference between (4.1.48) and (4.1.49) finds

$$\sigma_b = \frac{\delta E}{(3-4\upsilon)(1+\upsilon)} \tag{4.1.52}$$

where

$$\delta = -\frac{U_1 - U_2}{2R} \tag{4.1.53}$$

From (4.1.50) and (4.1.52), substitute the newly found coefficients into (4.1.45) and (4.1.46) thereby establishes

$$U = -\frac{\varepsilon R^2}{r} - \left(\frac{1-\upsilon}{3-4\upsilon}\right)\frac{4\delta R^2}{r}\cos 2\theta + \left(\frac{1}{3-4\upsilon}\right)\frac{\delta R^4}{r^3}\cos 2\theta \tag{4.1.54}$$

$$V = \left(\frac{1}{3-4\upsilon}\right)\frac{\delta R^4}{r^3}\sin 2\theta + \left(\frac{1-2\upsilon}{3-4\upsilon}\right)\frac{2\delta R^2}{r}\sin 2\theta \tag{4.1.55}$$

Having now determined the radial (U) and tangential (V) displacements that are in polar form, it is of practical use to transform the pair into rectangular components (x, z). In addition, hereinafter, the previous plate problem can now be viewed as a soil matrix and that x will denote the horizontal distances, and z for the vertical distance. At ground level or surface, $z = 0$. The open hole can now also be considered a bored tunnel as depicted in Figure 4.6.

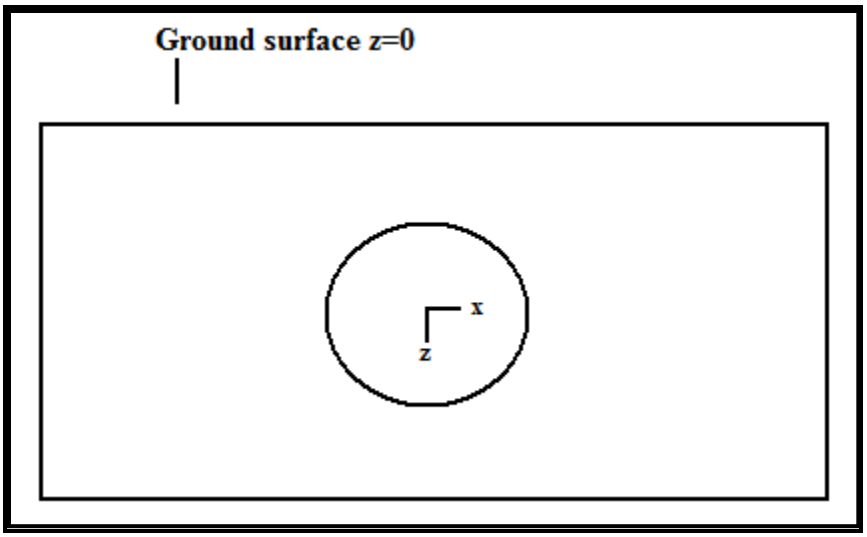

Fig.4.6 Plate problem from solid mechanics may now be viewed in the context of tunneling.

From linear algebra, a useful transformation rule that allows this conversion to take place can be defined as

$$\begin{bmatrix} u_x \\ u_Z \end{bmatrix} = \begin{bmatrix} \cos\theta & -\sin\theta \\ \sin\theta & \cos\theta \end{bmatrix} \begin{bmatrix} U \\ V \end{bmatrix} \tag{4.1.56}$$

The square matrix if replaced by the analytic components can take the form

$$\begin{bmatrix} u_x \\ u_z \end{bmatrix} = \begin{bmatrix} \frac{x}{r} & \frac{-z}{r} \\ \frac{z}{r} & \frac{x}{r} \end{bmatrix} \begin{bmatrix} U \\ V \end{bmatrix} \tag{4.1.57}$$

and now substituting for U and V obtains

$$\begin{bmatrix} u_x \\ u_z \end{bmatrix} = \begin{bmatrix} \frac{x}{r} & \frac{-z}{r} \\ \frac{z}{r} & \frac{x}{r} \end{bmatrix} \begin{bmatrix} -\frac{\varepsilon R^2}{r} - \left(\frac{1-\upsilon}{3-4\upsilon}\right)\frac{4\delta R^2}{r}\cos 2\theta + \left(\frac{1}{3-4\upsilon}\right)\frac{\delta R^4}{r^3}\cos 2\theta \\ \left(\frac{1}{3-4\upsilon}\right)\frac{\delta R^4}{r^3}\sin 2\theta + \left(\frac{1-2\upsilon}{3-4\upsilon}\right)\frac{2\delta R^2}{r}\sin 2\theta \end{bmatrix} \tag{4.1.58}$$

Expanding these matrices, the horizontal (u_x) and vertical (u_z) displacements were found to be

$$u_x = -\frac{\varepsilon R^2 x}{r^2} - \left(\frac{1-\upsilon}{3-4\upsilon}\right)\frac{4\delta R^2 x}{r}\left(\frac{x^2-z^2}{r^2}\right)\left(\frac{x}{r}\right) + \left(\frac{1}{3-4\upsilon}\right)\frac{\delta R^4}{r^3}\left(\frac{x^2-z^2}{r^2}\right)\left(\frac{x}{r}\right) - \frac{\delta R^4}{(3-4\upsilon)r^3}\left(\frac{2xz}{r^2}\right)\left(\frac{z}{r}\right) - \frac{2\delta R^2}{r}\left(\frac{1-2\upsilon}{3-4\upsilon}\right)\left(\frac{2xz}{r^2}\right)\left(\frac{z}{r}\right)$$

$$= -\frac{\varepsilon R^2 x}{r^2} - \left(\frac{1-\upsilon}{3-4\upsilon}\right)\frac{4\delta R^2 x}{r^4}\left(x^2-z^2\right) - \frac{\delta R^4 x}{(3-4\upsilon)r^6}\left(x^2-z^2\right) - \frac{2\delta R^4 x z^2}{(3-4\upsilon)r^6} - \left(\frac{1-2\upsilon}{3-4\upsilon}\right)\frac{4\delta R^2 x z^2}{r^4} \tag{4.1.59}$$

$$u_z = -\frac{\varepsilon R^2 z}{r^2} - \left(\frac{1-\upsilon}{3-4\upsilon}\right)\frac{4\delta R^2 z}{r^2}\left(\frac{x^2-z^2}{r^2}\right) + \left(\frac{1}{3-4\upsilon}\right)\frac{4\delta R^4 z}{r^4}\left(\frac{x^2-z^2}{r^2}\right) + \frac{\delta R^4 x}{(3-4\upsilon)r^4}\left(\frac{2xz}{r^2}\right) + \left(\frac{1-2\upsilon}{3-4\upsilon}\right)\frac{2\delta R^2 x}{r^2}\left(\frac{2xz}{r^2}\right)$$

$$= -\frac{\varepsilon R^2 z}{r^2} - \left(\frac{1-\upsilon}{3-4\upsilon}\right)\frac{4\delta R^2 z}{r^4}\left(x^2-z^2\right) + \frac{4\delta R^4 z}{(3-4\upsilon)r^6}\left(x^2-z^2\right) + \frac{2\delta R^4 x^2 z}{(3-4\upsilon)r^6} + \left(\frac{1-2\upsilon}{3-4\upsilon}\right)\frac{4\delta R^2 x^2 z}{r^4} \tag{4.1.60}$$

By applying the principle of virtual images as depicted in Figure 4.7, the single point at the sink was then projected symmetrically above the ground surface to produce the image. Hence, the singular displacements are represented as

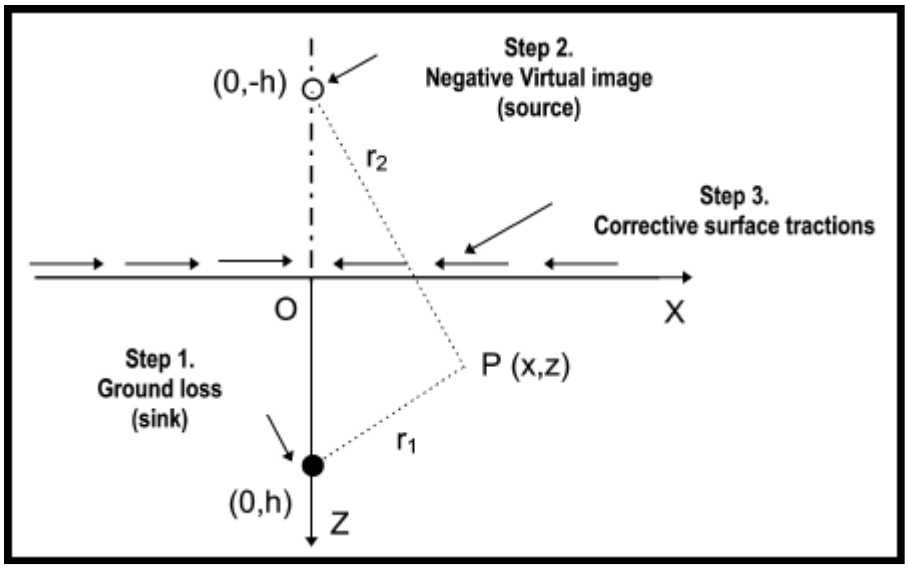

Fig.4.7 Application of the Sagaseta method. The sink and image points both cause displacements [5].

$$u_{x[1]} = -\varepsilon R^2 x\left(\frac{1}{r_1^2}+\frac{1}{r_2^2}\right)-\left(\frac{1-\upsilon}{3-4\upsilon}\right)4\delta R^2 x\left(\frac{x^2-z_1^2}{r_1^4}+\frac{x^2-z_2^2}{r_2^4}\right)$$
$$-\frac{\delta R^4 x}{3-4\upsilon}\left(\frac{x^2-z_1^2}{r_1^6}+\frac{x^2-z_2^2}{r_2^6}\right)-\frac{2\delta R^4 x}{(3-4\upsilon)}\left(\frac{z_1^2}{r_1^6}+\frac{z_2^2}{r_2^6}\right)-\left(\frac{1-2\upsilon}{3-4\upsilon}\right)4\delta R^2 x\left(\frac{z_1^2}{r_1^4}+\frac{z_2^2}{r_2^4}\right) \quad (4.1.61)$$

$$u_{z[1]} = -\varepsilon R^2\left(\frac{z_1}{r_1^2}+\frac{z_2}{r_2^2}\right)-\left(\frac{1-\upsilon}{3-4\upsilon}\right)4\delta R^2\left[z_1\left(\frac{x^2-z_1^2}{r_1^4}\right)+z_2\left(\frac{x^2-z_2^2}{r_2^4}\right)\right]$$
$$+\frac{4\delta R^4}{3-4\upsilon}\left[z_1\left(\frac{x^2-z_1^2}{r_1^6}\right)+z_2\left(\frac{x^2-z_2^2}{r_2^6}\right)\right] \quad (4.1.62)$$
$$+\frac{2\delta R^4 x^2}{(3-4\upsilon)}\left(\frac{z_1}{r_1^6}+\frac{z_2}{r_2^6}\right)+\left(\frac{1-2\upsilon}{3-4\upsilon}\right)4\delta R^2 x^2\left(\frac{z_1}{r_1^4}+\frac{z_2}{r_2^4}\right)$$

Here ε is defined by (4.1.51) and δ by (4.1.53). In tunnel engineering, ε is called the radial strain or ground loss, and δ is referred to as a distortion or ovalizaton parameter. In addition, the new *r* and *z* distance terms are defined by

$$\left.\begin{aligned} z_1 &= z - h \\ z_2 &= z + h \\ r_1^2 &= x^2 + z_1^2 \\ r_2^2 &= x^2 + z_2^2 \end{aligned}\right\} \tag{4.1.63}$$

Components with the sub-indices 1 denotes the lower plane while 2 indicates the upper plane. The *h* in (4.1.63) may be considered the tunnel placement depth measured from the center of the opening to the ground surface and *x* denotes the lateral distance from the center of the cavity.

Based on the derived information so far, it is now worthwhile to develop a stress formula acting normal at the ground level ($z = 0$) in which the pressure is influenced internally from the tunnel cavity. In turn, displacements may be found as suggested by Verruijt and Booker which made use of Fourier methods [26, 29]. This normal stress σ_{zz} may be determined by applying the transformation rule

$$\sigma_{zz} = \sigma_r \sin^2\theta + \sigma_\theta \cos^2\theta + \tau_{r\theta} \sin 2\theta \tag{4.1.64}$$

From above, the modified radial, tangential and shear stress are restated as follows

$$\sigma_r = \frac{\varepsilon E}{(1+\upsilon)}\left(1 - \frac{R^2}{r^2}\right) + \frac{\delta E}{(3-4\upsilon)(1+\upsilon)}\left(1 + \frac{3R^4}{r^4} - \frac{4R^2}{r^2}\right)\cos 2\theta \tag{4.1.65}$$

$$\sigma_\theta = \frac{\varepsilon E}{(1+\upsilon)}\left(1 + \frac{R^2}{r^2}\right) - \frac{\delta E}{(3-4\upsilon)(1+\upsilon)}\left(1 + \frac{3R^4}{r^4}\right)\cos 2\theta \tag{4.1.66}$$

$$\tau_{r\theta} = -\frac{\delta E}{(3-4\upsilon)(1+\upsilon)}\left(1-\frac{3R^4}{r^4}+\frac{2R^2}{r^2}\right)\sin 2\theta \tag{4.1.67}$$

When these expressions are expanded and retained for the higher order terms, the equations becomes

$$\sigma_r = -\frac{2\varepsilon R^2 G}{r^2}+\frac{6\delta R^4 G}{\lambda r^4}\cos 2\theta-\frac{8\delta R^2 G}{\lambda r^2}\cos 2\theta \tag{4.1.68}$$

$$\sigma_\theta = \frac{2\varepsilon R^2 G}{r^2}-\frac{6\delta R^4 G}{\lambda r^4}\cos 2\theta \tag{4.1.69}$$

$$\tau_{r\theta} = \frac{6\delta R^4 G}{\lambda r^4}\sin 2\theta-\frac{4\delta R^2 G}{\lambda r^2}\sin 2\theta \tag{4.1.70}$$

where G denotes the shear modulus and $\lambda = 3-4\upsilon.$ Now, the normal stress is written out in analytic form as

$$\sigma_{zz} = -\frac{2\varepsilon R^2 GR\left(h^2-x^2\right)}{\left(x^2+h^2\right)^2}-\frac{8\delta R^2 G\left(3x^2h^2-h^4\right)}{\lambda\left(x^2+h^2\right)^3}-\frac{6\delta R^4 G}{\lambda\left(x^2+h^2\right)^4}\left(-6h^2x^2+h^4+x^4\right) \tag{4.1.71}$$

Applying the principle of virtual image doubles the result of (4.1.71) thereby obtains

$$\sigma_{zz} = -\frac{4\varepsilon R^2 G\left(h^2-x^2\right)}{\left(x^2+h^2\right)^2}-\frac{16\delta R^2 G\left(3h^2x^2-h^4\right)}{\lambda\left(x^2+h^2\right)^3}-\frac{12\delta R^4 G}{\lambda\left(x^2+h^2\right)^4}\left(-6h^2x^2+h^4+x^4\right) \tag{4.1.72}$$

In passing, it should be noted that there are no shear stresses, that is $\tau_{zx} = 0$ and vertical displacement at the surface in the real sense. The former may be confirmed by applying the shear stress law

$$\tau_{zx} = \frac{1}{2}\left(\sigma_r - \sigma_\theta\right)\sin 2\theta + \tau_{r\theta}\cos 2\theta \tag{4.1.73}$$

and when inserting the polar stress coefficients of (4.1.68), (4.1.69) and (4.1.70), attention is made to the fact that *p* and *q* are zero in evaluating for σ_a and σ_b. The latter statement could be verified by inserting *z* = 0 into (4.1.62) which makes $u_{z[1]}$ zero.

In order to obtain the displacements needed to counterbalance in the opposite direction of the acting normal stress, one possible method made use of the Fourier cosine transform $F_c\left(a\right)$. The justification of $F_c\left(a\right)$ has to do with the fact that (4.1.72) is an even function. In the treatise by Sneddon [26], the horizontal and vertical displacement may be represented as

$$u_{x[2]} = -\frac{1}{G\pi}\int_0^\infty P\left(a\right)\exp\left(-az\right)\left[\left(1-2\upsilon-az\right)\right]\frac{\sin\left(ax\right)}{a}da \tag{4.1.74}$$

$$u_{z[2]} = \frac{1}{G\pi}\int_0^\infty P\left(a\right)\exp\left(-az\right)\left[2\left(1-\upsilon\right)+az\right]\frac{\cos\left(ax\right)}{a}da \tag{4.1.75}$$

where *G* denotes the shear modulus and $P\left(a\right)$ can be defined as

$$P\left(a\right) = -\int_0^\infty \sigma_{zz}\cos\left(ax\right)dx \tag{4.1.76}$$

or by inserting (4.1.72) obtains

$$P(a)=\int_0^{\infty}\left[\begin{array}{l}\dfrac{4\varepsilon R^2G\left(h^2-x^2\right)}{\left(x^2+h^2\right)^2}+\dfrac{16\delta R^2G\left(3x^2h^2-h^4\right)}{\lambda\left(x^2+h^2\right)^3}\\ \qquad\qquad+\dfrac{12\delta R^4G}{\lambda\left(x^2+h^2\right)^4}\left(-6h^2x^2+h^4+x^4\right)\end{array}\right]\cos(ax)dx \tag{4.1.77}$$

In the integrands of (4.1.74) and (4.1.75), use of $n=\dfrac{1}{1-2\upsilon}$ was made to simplify the expressions to

$$u_{x[2]}=-\frac{1}{G\pi}\int_0^{\infty}P(a)\exp(-az)\left[\frac{1-naz}{n}\right]\frac{\sin(ax)}{a}da \tag{4.1.78}$$

$$u_{z[2]}=\frac{1}{G\pi}\int_0^{\infty}P(a)\exp(-az)\left[\frac{1+n+naz}{n}\right]\frac{\cos(ax)}{a}da \tag{4.1.79}$$

The evaluation of *P(a)* could be determined first by separating the integrand of Eq. (4.1.77) into three sub- components, and by referring to any mathematical table [27] for the particular Fourier cosine transform of

$$F_c\left[\frac{1}{x^2+h^2}\right]=\frac{\pi\exp(-ah)}{2h} \tag{4.1.80}$$

The next step required a series of single or multiple partial differentiations with respect to either variables *a* or *h* for both sides of (4.1.80) and then finally adds up all parts to attain the final result for all terms of (4.1.77). These sequences of steps could be traced out as shown in Figure 4.8.

Term	Differentiation Order
$-4\varepsilon R^2 G\int_0^\infty \frac{h^2\cos(ax)dx}{\left(x^2+h^2\right)^2}$	$\frac{\partial}{\partial h}$
$4\varepsilon R^2 G\int_0^\infty \frac{x^2\cos(ax)dx}{\left(x^2+h^2\right)^2}$	$\frac{\partial}{\partial h}\rightarrow\frac{\partial^2}{\partial a^2}\left(\frac{\partial}{\partial h}\right)$
$-\frac{16\delta R^2 G}{\lambda}\int_0^\infty \frac{3h^2x^2\cos(ax)dx}{\left(x^2+h^2\right)^3}$	$\frac{\partial^2}{\partial h^2}\rightarrow\frac{\partial^2}{\partial a^2}\left(\frac{\partial^2}{\partial h^2}\right)$
$\frac{16\delta R^2 G}{\lambda}\int_o^\infty \frac{h^4\cos(ax)dx}{\left(x^2+h^2\right)^3}$	$\frac{\partial^2}{\partial h^2}$
$\frac{12\delta R^4 G}{\lambda}\int_0^\infty \frac{6h^2x^2\cos\left(ax\right)dx}{\left(x^2+h^2\right)^4}$	$\frac{\partial^3}{\partial h^3}\rightarrow\frac{\partial^2}{\partial a^2}\left(\frac{\partial^3}{\partial h^3}\right)$
$-\frac{12\delta R^4 G}{\lambda}\int_0^\infty \frac{h^4\cos\left(ax\right)dx}{\left(x^2+h^2\right)^4}$	$\frac{\partial^3}{\partial h^3}$
$-\frac{12\delta R^4 G}{\lambda}\int_0^\infty \frac{x^4\cos\left(ax\right)dx}{\left(x^2+h^2\right)^4}$	$\frac{\partial^3}{\partial h^3}\rightarrow\frac{\partial^4}{\partial a^4}\left(\frac{\partial^3}{\partial h^3}\right)$

Fig.4.8 Differentiation summary for the Fourier cosine transform to evaluate *P(a).*

In Appendix A, all the calculations are shown. When all simplifications are made, the final integrals should have the following forms

$$4\varepsilon R^2 G\int_0^\infty \frac{\left(h^2-x^2\right)\cos axdx}{\left(x^2+h^2\right)^2}=2\varepsilon R^2 G\pi a\exp\left(-ah\right) \tag{4.1.81}$$

$$\frac{16\delta R^2 G}{\lambda}\int_0^\infty \frac{\left(3h^2x^2-h^4\right)\cos axdx}{\left(x^2+h^2\right)^3}=\frac{2\delta R^2 G\pi a^2 h\exp\left(-ah\right)}{\lambda} \tag{4.1.82}$$

$$\frac{12\delta R^4 G}{\lambda}\int_0^\infty \frac{\left(-6h^2x^2+h^4+x^4\right)\cos axdx}{\left(x^2+h^2\right)^4}=\frac{\delta R^4 G\pi a^3\exp\left(-ah\right)}{\lambda} \tag{4.1.83}$$

and by combining (4.1.81) through (4.1.83) according to (4.1.77) will obtain the determination for *P(a)* as

$$P(a) = 2\varepsilon R^2 G\pi a \exp(-ah) + \frac{2\delta R^2 G\pi a^2 h}{\lambda} \exp(-ah) + \frac{\delta R^4 G\pi \exp a^3(-ah)}{\lambda} \tag{4.1.84}$$

The last step in establishing the two directional displacement equations were then to insert (4.1.84) into (4.1.78) and (4.1.79). In the next computation process, additional Fourier sine $F_s[a]$ and cosine $F_c[a]$ transforms below must be considered as follows

$$F_s\left[\exp(-az)\right] = \frac{x}{x^2 + z^2} \tag{4.1.85}$$

$$F_s\left[a^{b-1}\exp(-az)\right] = \frac{\Gamma(b)\sin\left(b\arctan\dfrac{x}{z}\right)}{\left(x^2+z^2\right)^{b/2}} \tag{4.1.86}$$

$$F_c\left[\exp(-az)\right] = \frac{z}{x^2 + z^2} \tag{4.1.87}$$

$$F_c\left[a^{b-1}\exp(-az)\right] = \frac{\Gamma(b)\cos\left(b\arctan\dfrac{x}{z}\right)}{\left(x^2+z^2\right)^{b/2}} \tag{4.1.88}$$

where Γ(b) denotes the gamma function [27]. In particular, when verified in analytical detail [see Appendix B], the following transforms will serve as identities ready for algebraic expansion

$$F_s\left[\exp(-az_2)\right] = \frac{x}{r_2^2} \tag{4.1.89}$$

$$F_s\left[a\exp\left(-az_2\right)\right]=\frac{2xz_2}{r_2^4} \tag{4.1.90}$$

$$F_s\left[a^2\exp\left(-az_2\right)\right]=\frac{2x^3+6xz_2}{r_2^6} \tag{4.1.91}$$

$$F_s\left[a^3\exp\left(-az_2\right)\right]=\frac{16x^3z_2+24xz_2^3}{r_2^8} \tag{4.1.92}$$

$$F_c\left[\exp\left(-az_2\right)\right]=\frac{z_2}{r_2^2} \tag{4.1.93}$$

$$F_c\left[a\exp\left(-az_2\right)\right]=-\frac{\left(x^2-z_2^2\right)}{r_2^4} \tag{4.1.94}$$

$$F_c\left[a^2\exp\left(-az_2\right)\right]=-\frac{2z_2}{r_2^6}\left(3x^2-z_2^2\right) \tag{4.1.95}$$

$$F_c\left[a^3\exp\left(-az_2\right)\right]=\frac{6}{\left(x^2+z_2^2\right)^2}-\frac{48z_2^2}{\left(x^2+z_2^2\right)^3}+\frac{48z_2^4}{\left(x^2+z_2^2\right)^4} \tag{4.1.96}$$

Making the insertion of (4.1.84) into (4.1.78) gets the following general expression

$$u_{x[2]}=-\frac{P(a)}{G\pi}\left[\frac{1}{n}\int_0^\infty\exp\left(-az\right)\frac{\sin\left(ax\right)}{a}da-z\int_0^\infty a\exp\left(-ax\right)\frac{\sin\left(ax\right)}{a}da\right] \tag{4.1.97}$$

Using the identities from (4.1.89) to (4.1.92) establishes the explicit result for (4.1.97) as

$$u_{x[2]} = -\frac{2\varepsilon R^2}{n} F_s\left[\exp\left(-az_2\right)\right] - \frac{2\delta R^2 h}{n\lambda} F_s\left[a\exp\left(-az_2\right)\right] - \frac{\delta R^4}{n\lambda} F_s\left[a^2\exp\left(-az_2\right)\right]$$
$$+z\left(2\varepsilon R^2 F_s\left[a\exp\left(-az_2\right)\right] + \frac{2\delta R^2 h}{\lambda} F_s\left[a^2\exp\left(-az_2\right)\right] + \frac{\delta R^4}{\lambda} F_s\left[a^3\exp\left(-az_2\right)\right]\right)$$

(4.1.98)

and when expanded gets

$$u_{x[2]} = -2\varepsilon R^2\left(1-2\upsilon\right)\frac{x}{x^2+z_2^2} - 4\delta R^2 hx\frac{\left(1-2\upsilon\right)}{\left(3-4\upsilon\right)}\frac{z_2}{\left(x^2+z_2^2\right)^2} - \left(\frac{1-2\upsilon}{3-4\upsilon}\right)\delta R^4\left[\frac{2x^3+6xz_2^2}{\left(x^2+z_2^2\right)^3}\right]$$
$$+4\varepsilon R^2\frac{xzz_2}{\left(x^2+z_2^2\right)^2} + \frac{2\delta R^2 hz}{3-4\upsilon}\left[\frac{2x^3+6xz_2^2}{\left(x^2+z_2^2\right)^3}\right] + \left(\frac{1-2\upsilon}{3-4\upsilon}\right)\delta R^4 z\left[\frac{16x^3 z_2+24xz_2^3}{\left(x^2+z_2^2\right)^4}\right]$$

(4.1.99)

Similarly, the substitution of (4.1.84) into (4.1.79) obtains the general expression

$$u_{z[2]} = \frac{P\left(a\right)}{G\pi}\left[\beta\int_0^\infty \exp\left(-az\right)\frac{\cos\left(ax\right)}{a}da + z\int_0^\infty a\exp\left(-az\right)\frac{\cos\left(ax\right)}{a}da\right] \qquad (4.1.100)$$

and inserting the identities from (4.1.93) to (4.1.96) into (4.1.100) gets

$$u_{z[2]} = 2\beta\varepsilon R^2 F_c\left[\exp\left(-az_2\right)\right] + F_c\left[a\exp\left(-az_2\right)\right] + \frac{\beta\delta R^4}{\lambda}F_c\left[a^2\exp\left(-az_2\right)\right]$$
$$+z\left(2\varepsilon R^2 F_c\left[a\exp\left(-az_2\right)\right] + \frac{2\delta R^2 h}{\lambda}F_c\left[a^2\exp\left(-az_2\right)\right] + \frac{\beta\delta R^4}{\lambda}F_c\left[a^3\exp\left(-az_2\right)\right]\right)$$

(4.1.101)

where $\beta = \frac{1+n}{n}$ which is also equal to $2\left(1-\upsilon\right)$. Expanding (4.1.101) obtains

$$u_{z[2]} = 4(1-\upsilon)\varepsilon R^2 \frac{z_2}{x^2+z_2^2} - \frac{4(1-\upsilon)\delta R^2 h}{(3-4\upsilon)}\left[\frac{x^2-z_2^2}{\left(x^2+z_2^2\right)^2}\right] - \frac{4(1-\upsilon)\delta R^4}{(3-4\upsilon)}\left[z_2\frac{3x^2-z_2^2}{\left(x^2+z_2^2\right)^3}\right]$$
$$- 2\varepsilon R^2 z\left[\frac{x^2-z_2^2}{\left(x^2+z_2^2\right)^2}\right] - \frac{4\delta R^2 hz}{3-4\upsilon}\left[z_2\frac{3x^2-z_2^2}{\left(x^2+z_2^2\right)^3}\right]$$
$$+ \frac{2(1-\upsilon)}{3-4\upsilon}\delta R^4 z\left[\frac{6}{\left(x^2+z_2^2\right)^2} - \frac{48z_2^2}{\left(x^2+z_2^2\right)^3} + \frac{48z_2^4}{\left(x^2+z_2^2\right)^4}\right] \tag{4.1.102}$$

The complete solution was defined at the start by (4.1.1) and (4.1.2) which stated the sum of the real and virtual components for the individual horizontal and vertical directions respectively. Thus, the displacement equations could be re-written to include the derived information as

$$u_x = u_{x[1]}(4.1.61) + u_{x[2]}(4.1.99) \tag{4.1.103}$$

$$u_z = u_{z[1]}(4.1.62) + u_{z[2]}(4.1.102) \tag{4.1.104}$$

For the special case of surface deflections, insert $z = 0$ into $z_2 = z + h$ and Eq. (4.1.104) becomes

$$u_{z(0)} = 4(1-\upsilon)\varepsilon R^2 \frac{h}{x^2+h^2} - \frac{4(1-\upsilon)\delta R^2 h}{(3-4\upsilon)}\left[\frac{x^2-h^2}{\left(x^2+h^2\right)^2}\right] - \frac{4(1-\upsilon)\delta R^4 h}{(3-4\upsilon)}\left[\frac{3x^2-h^2}{\left(x^2+h^2\right)^3}\right] \tag{4.1.105}$$

This was the subsidence equation used for the analysis of normalized terms.

4.2 Normalized Representation

As was stated in Eq. (4.1.105), two higher-order terms were associated with the ovalization factor. The first term could be normalized to become

$$\frac{u_z h}{\delta R^2} = \frac{\left(\frac{x}{h}\right)^2 - 1}{\left[1 + \left(\frac{x}{h}\right)^2\right]^2} \tag{4.2.1}$$

and the second term represented as

$$\frac{u_z h^3}{\delta R^4} = \frac{3\left(\frac{x}{h}\right)^2 - 1}{\left[1 + \left(\frac{x}{h}\right)^2\right]^3} \tag{4.2.2}$$

These normalized representations were plotted and discussed in Chapter 5. Each normalized term is a non-dimensional number analogous to an aspect ratio or Reynold's number. These numbers have no units and were intended to ascertain any behavioural or qualitative patterns of the subsidence with respect to the lateral position of the tunnel centerline. In this case, for the ratio $\frac{x}{h}$, h may be considered fixed while x could indicate any horizontal location away from the tunnel.

Chapter 5 Application of Methods

5.1 Introduction

The g parameter outlined in Chapter 2 is described in detail so as to demonstrate its usefulness in connection with the derived radial strain and ovalization of Chapter 4. An expression is given to link these parameters. In addition, a numerical example is discussed using tunneling data from a published paper and making use of the derived subsidence equation (4.1.105). Finally, some qualitative features of the Eq. (4.1.105) are examined so as to obtain some prediction characteristics for expecting settlement responses during shallow tunnel excavation.

5.2 Determination of Physical Gap (G_p)

The physical gap has been defined as the difference between the vertical distances of the shield (D) and lining (d) crown. The vertical distance of the shield is taken from the rear rather than at the face of the TBM because in the case (iii) scenario, the shield part may have rotated. As shown in Figure 5.1, the sub-components of the shield diameter indicate an equivalent definition for determining G_p. Here, the totality of the shield diameter consisted of the lining distance, lining clearance (δ) and tailpiece thickness (Δ). Since the tailpiece thickness is both located at the crown (top) and base (bottom), the actual thickness becomes 2Δ. The sum of δ and 2Δ is then the equivalent formula for the physical gap as stated in Eq. (5.2.1).

$$G_p = D - d = \delta + 2\Delta \tag{5.2.1}$$

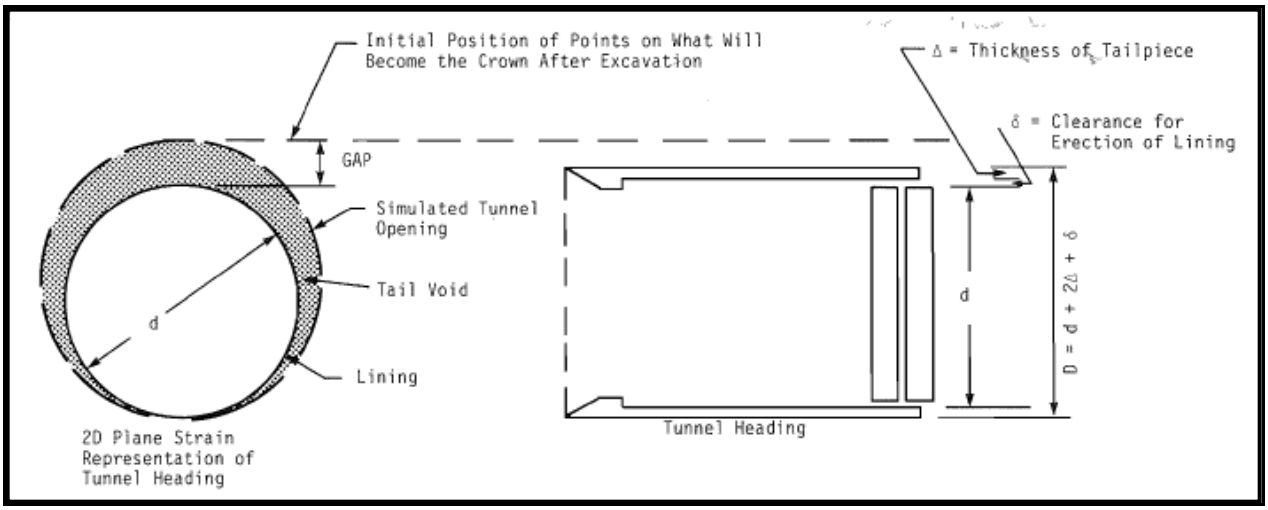

Fig.5.1 Measurement points for determining the physical gap (Gp) during tunnel excavation [13].

5.3 Determination of Spatial Deformation $\left(u_{3D}^{*}\right)$

As a result of interface contact of the TBM and soil at the front, stresses applied on the face will often cause significant soil intrusion. These horizontal displacements occurring at the face of the TBM contribute to a volume loss, and thus an additional term was needed in Eq. (2.2.1). Such a term was designated a spatial deformation and may be quantified based on two or three dimensional finite element studies. Lee et al. asserted that the two dimensional term can replace the spatial quantity without precision loss towards the deformational calculation. Determining the value u_{3D}^{*} requires evaluating two quantities which are based on FEM and prepared charts. The equation for the spatial deformation is given as

$$u_{3D}^{*} = \frac{k_1 \delta_x}{2} \tag{5.3.1}$$

where k_1 is a special factor characterizing soil intrusion across the tunnel face. It too may be defined as a ratio

$$k_1 = \frac{\text{Vol. (non-uniform axial intrusion) using 3D FEM}}{\text{Vol. (uniform axial intrusion)}} \tag{5.3.2}$$

but in published studies, fall in the range between 0.7 to 0.9 for stiff to soft clays. However, k_1 = 1 may be safely used [13].

The δ_x is called the tunnel face intrusion and may be estimated with (5.3.3) for some stability ratio N and finally back calculate to find δ_x. As suggested by Lee et al., an N-Ω chart may be prepared to organize a series of standard values so the designer may simply read it off to begin the calculations. The vertical axis makes use of the non-dimensional ratio given by

$$\Omega = \frac{\delta_x E}{R P_o} \tag{5.3.3}$$

where E is the elastic modulus of the soil, R is the tunnel radius, and P_o is the total stress removed at the tunnel face calculated using

$$P_o = \left(K_o' P_v' + P_w\right) - P_i \tag{5.3.4}$$

with K_o' representing the effective coefficient earth pressure at rest, P_v' as the vertical effective stress at the tunnel spring line (side), P_w denoting the porewater pressure and P_i as the tunnel

supporting pressure. The value of P_i may be zero if the tunnel is completely bored and if found at the tunnel face is compressed air will make P_i greater than zero.

5.4 Determination of Workmanship (ω)

The need for the workmanship term ω addresses the case (iii) of Figure 2.3 with respect to the complex nature of the tunnel pathway and how the TBM must deal with such a situation. In this construction scenario, the tunnel shield must either be steered vertically up or down resulting in additional material being excavated. In addition, the decision to include lining installation behind the shield and external components to reduce frictional drag may be factored in the final workmanship value (Figure 5.2).

A way of quantifying this particular loss has its origins from the work of Cording and Hansmire [13]. The authors suggested on top of the shield, a point over the crown would displace an amount equal to the length of the shield multiplied by the excessive pitch of the shield. This concept may be put into equation form as

$$V_{shield} = \pi RL \times ExcessPitch \tag{5.4.1}$$

where R is the tunnel radius, L is the length of the shield and the Excess Pitch may be measured based on the schematic of Figure 5. An alternative formulation is to view the transverse section composed of the TBM diameter $2R$ and adding the excess above the crown designated as ω to form a total length of $2R+\omega$. Then substituting into Eq. (5.4.1) will get

$$V_{shield} = \pi\left(R + \frac{\omega}{2}\right)^2 - \pi R^2 \tag{5.4.2}$$

If higher order terms are ignored in Eq. (5.2) when expanded, then it may be simplified to

$$V_s = \pi R\omega \tag{5.4.3}$$

where $\omega = L \times ExcessPitch$ and the value of the excess pitch is decided beforehand.

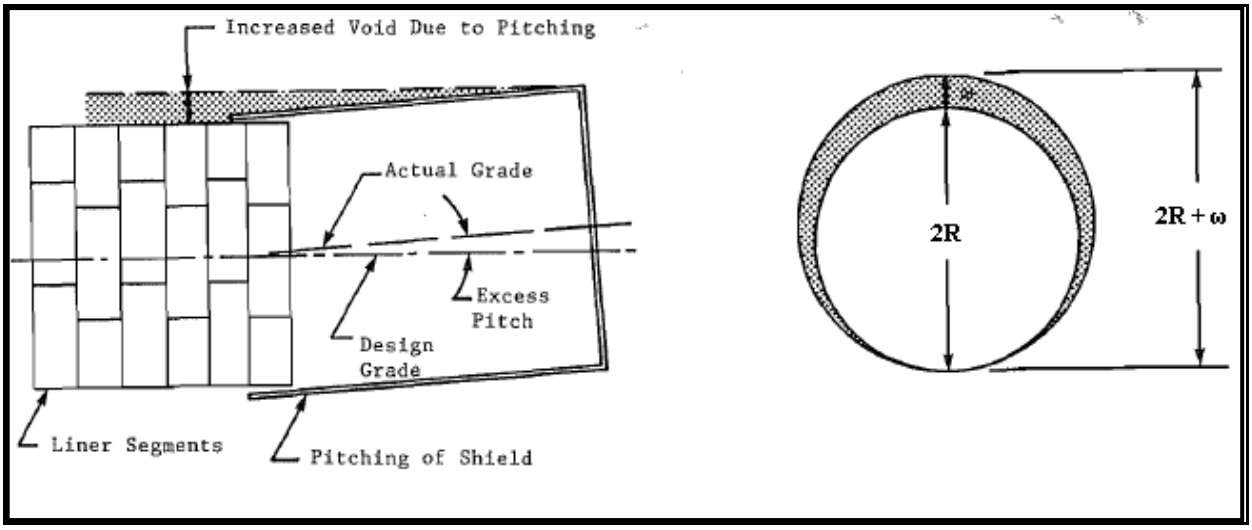

Fig.5.2 Workmanship term accounts for potential tilting of the tunnel shield [13].

Even with control of the tunnel face to proceed with pitch irregularity, the TBM may also have some side to side motion as well to complicate the precise value of ω. This combination of erratic movement will cause over-excavated voids thus allowing radial ground loss to form. Two potential cases were modelled by Lee et al. to quantify this particular ground loss and has to do with either there are unlining or lining installations begins behind the shield.

For the unlined case, ω was proposed to be calculated using

$$\omega = \frac{u_i}{3} \tag{5.4.4}$$

where u_i is the elastoplastic plane strain displacement at the crown and may be determined by applying

$$\frac{u_i}{R} = 1 - \sqrt{\frac{1}{1 + \frac{2c_u\left(1+\nu_u\right)\left[\exp\left(\frac{N-1}{2}\right)\right]^2}{E_u}}} \tag{5.4.5}$$

Here, E_u and ν_u are the undrained elastic modulus and Poisson's ratio, R is the tunnel radius, c_u is the undrained soil strength, and N is a stability number.

An alternative case incorporates lining and as such may be estimated by using

$$\omega = 0.6G_p \tag{5.4.6}$$

but only if (2.2.3.6) satisfies the following inequality

$$\omega_{Eq(5.4.7)} \leq \omega_{Eq(5.4.4)} \tag{5.4.7}$$

If the inequality of (5.4.7) has not been met, then the governing value of ω must be based on Eq. (5.4.4).

One last factor can further refine ω which addresses frictional contact influence between the soil and shield interface. It has been identified that ground losses can be created from the welded beads on the hood for the intent of minimizing friction as the shield moves forward and

provide more steering flexibility. With this bead attachment, the workmanship term defined by the governing result of Eq. (5.4.7) may be represented as

$$\omega = \left(\text{Value determined by Eq. (5.4.7)}\right) + nt_b \tag{5.4.8}$$

where t_b is the bead thickness and n may be considered by deciding which of the following three cases are applicable

$$n = \begin{cases} 0 \Rightarrow \text{no bead} \\ 1 \Rightarrow \text{bead spans the upper } 180^o \text{ of hood} \\ 2 \Rightarrow \text{bead covers full circumference of hood and shield} \end{cases}$$

5.5 Linkage of Parameters

A simple relation is demonstrated so as to bridge the gap parameter discussed above and the parameters radial strain and ovalization. This technique connects the data measured from the field with the analytical equations. By taking the ratio $\frac{\sigma_b}{\sigma_a}$ and using Eqs. (4.43), (4.44), (4.50) and (4.52) for simplification, it can be established that $\frac{\delta}{\varepsilon} = \left(3 - 4\upsilon\right)\frac{p-q}{p+q}$. The term $\frac{p-q}{p+q}$ is also equivalently defined by $\frac{1-\sin\phi}{1+\sin\phi}$ from the Mohr-Coulomb theory of soil failure [6]. In this case, ε is related to g if g<<R, then g is approximately $2u_0$ where u_o is the amount of radial displacement. Then $\varepsilon = \frac{2u_0}{R} = \frac{g}{R}$ which forms the linkage between ε and g.

5.6 Numerical Example

Having described the theoretical aspects of determining ground level subsidence caused by shallow tunnel operations, it is quite useful to compute the quantity using a published example where an actual excavation project has taken place. The example taken is from [17] and the subsidences calculated here include only Section 1 for discussion.

Since four methods (Peck, Sagaseta, Verruijt-Booker, and thesis) were used for comparison, the data consisted of the inflection point i = 6.3 m, R = 4.7 m, h = 14.2 m, ε = 0.0018, δ = 0.0023, υ = 0.3, g = 0.012 m and V_s = 0.50 percent. The normalized settlement profiles for the right side of the tunnel are displayed in Figure 5.3. A parametric analysis may be conducted using the plotted information in order to determine any significant changes if a variable of interest were to be altered. The discussion of such a study is presented in the next section.

The lowest subsidence (11.2 mm) estimate came from Sagaseta's original formula while the highest settlement (32.2 mm) was obtained using the Peck equation. The thesis-derived equation obtained a deflection value close to the Verruijt-Booker solution. Despite that the different final form of the subsidence equations used, the end result all resemble a normal curve distribution. In testing the ε-g relation, the equation predicted a value of ε = 0.0025 compared to the measured 0.0018 which has a relative error of 40 percent.

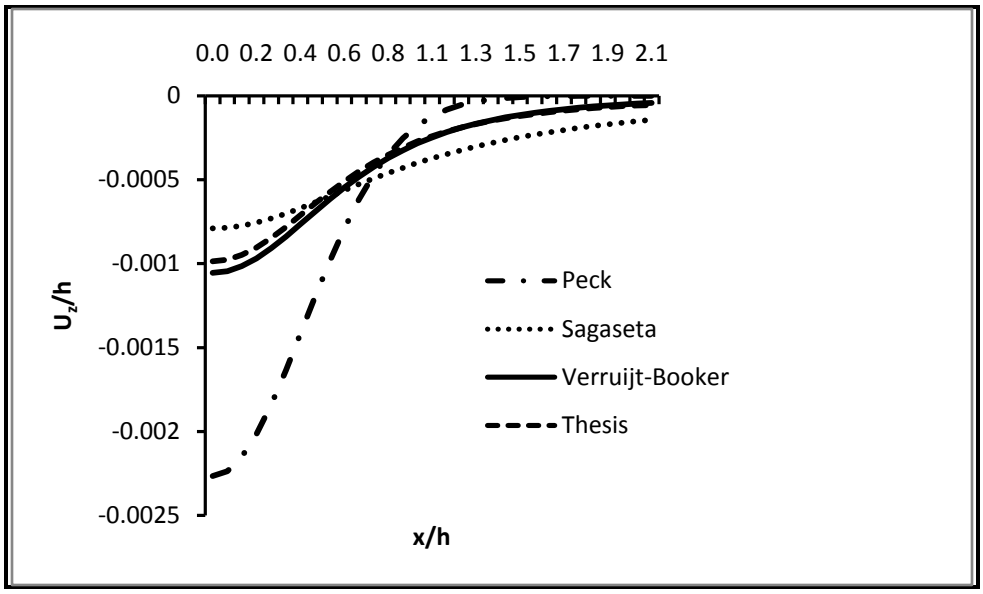

Fig.5.3 Normalized settlement distribution based on four different methods.

5.7 Parametric Analysis

The numerical example described in the previous section suggests a parametric study could be obtained. In particular, the placement depths of the tunnel may be altered to gain some information regarding any changes of the subsidence from the four methods discussed.

A total of 5 plotted graphs examined the distributions for depths between 20 to 40 m are shown in Figures 5.4 to 5.8. These additional graphed figures including Figure 5.3 demonstrated a common behaviour in that the settlements over the tunnel decreased if deeper depths were chosen for construction. The Peck method however retained its distinctive bell-curve shape throughout the comparison while the other three methods showed a flattened pattern progression from shallow to deeper zones.

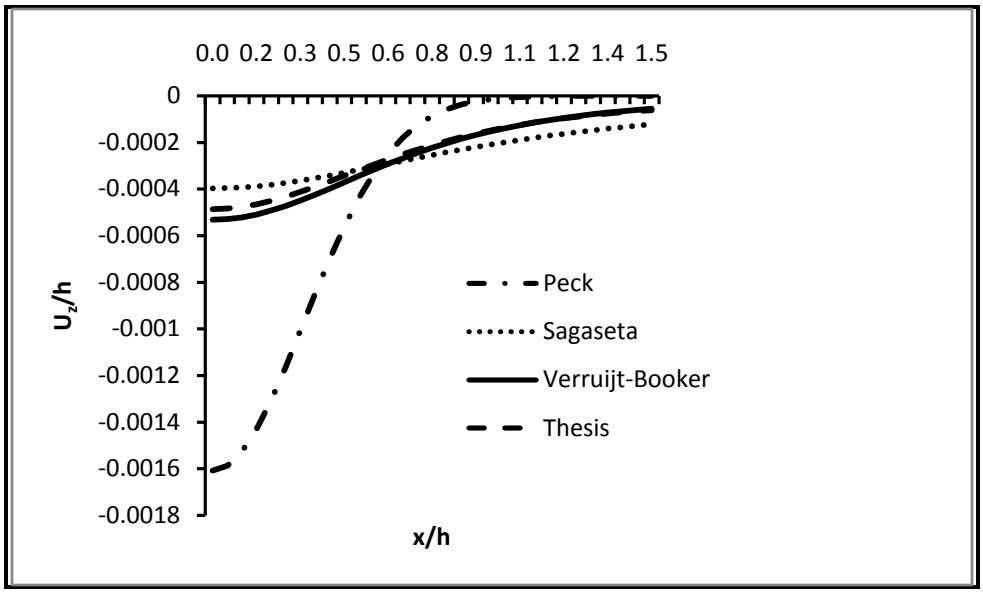

Fig.5.4 Subsidence distribution based on depth of 20 meters.

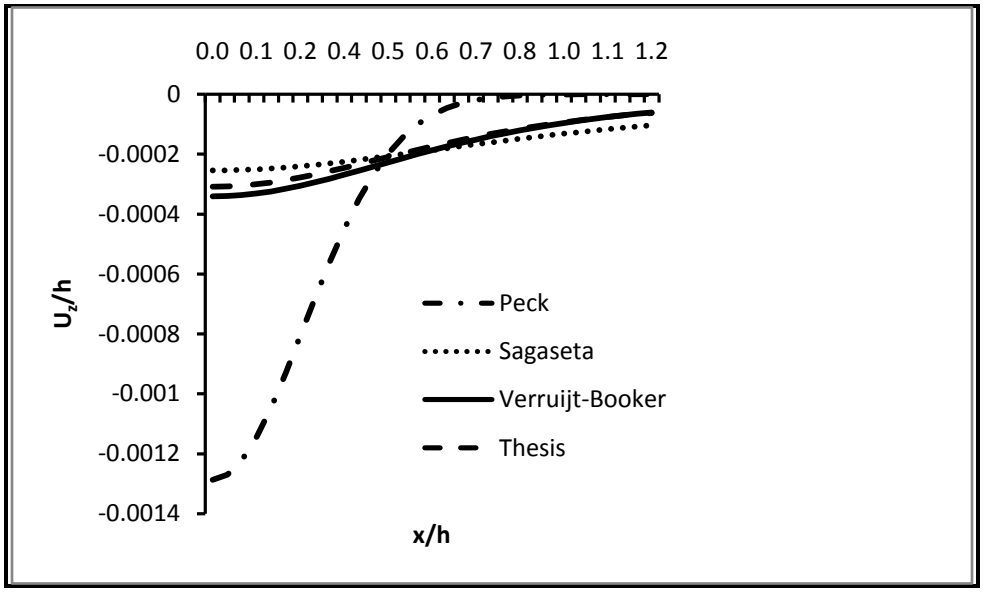

Fig.5.5 Subsidence distribution based on depth of 25 meters.

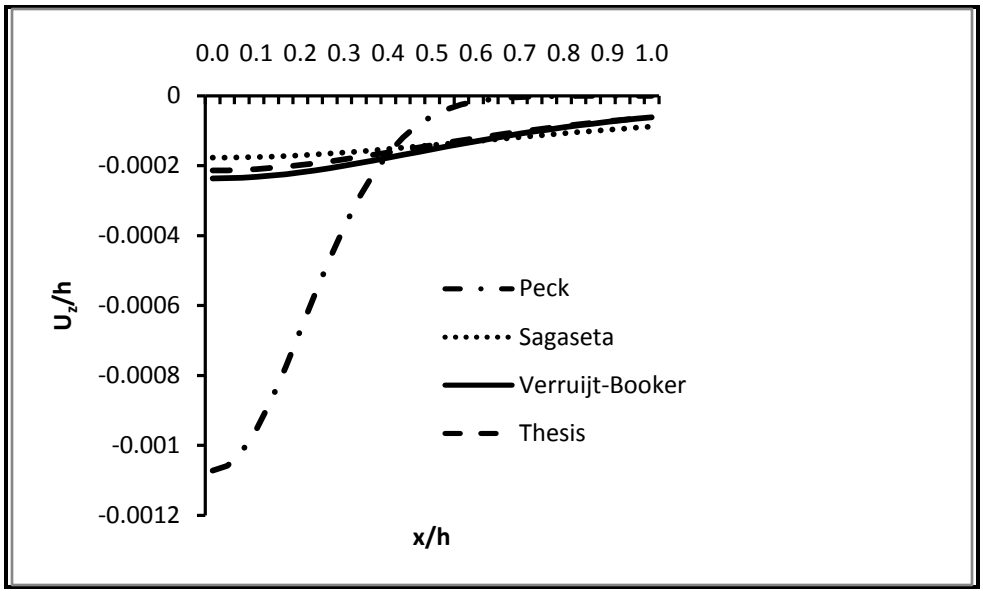

Fig.5.6 Subsidence distribution based on depth of 30 meters.

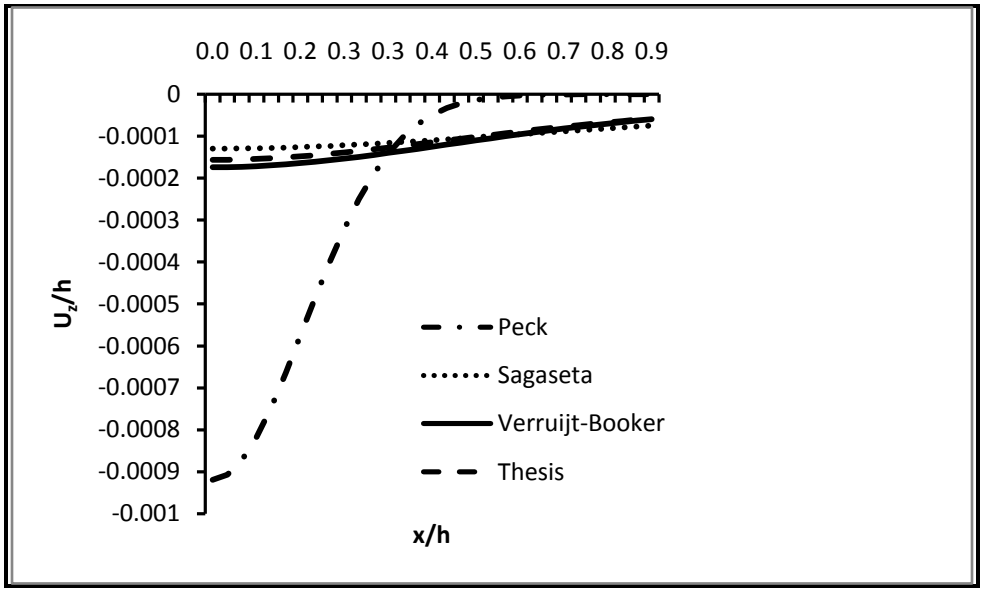

Fig.5.7 Subsidence distribution based on depth of 35 meters.

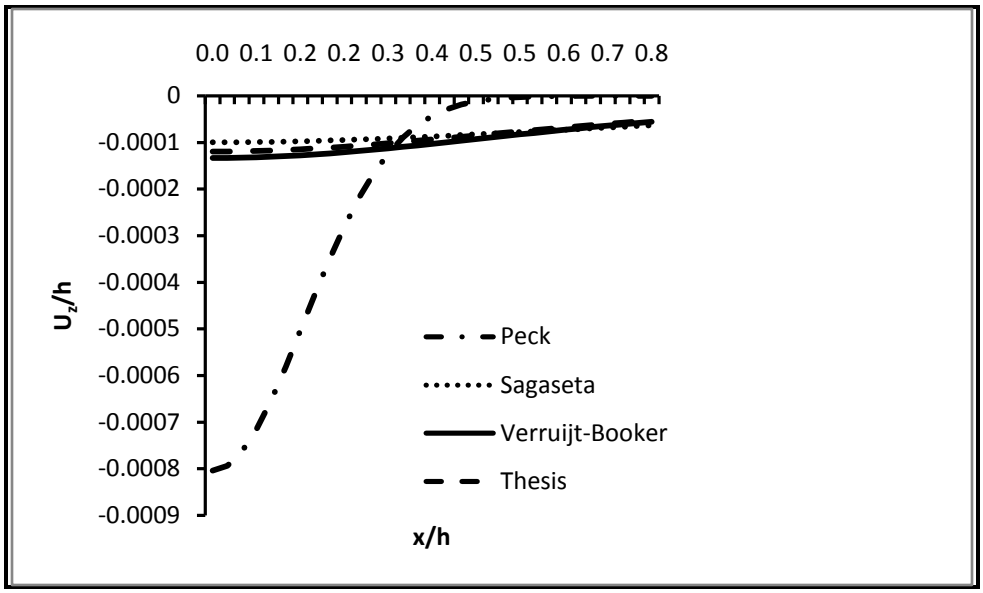

Fig.5.8 Subsidence distribution based on depth of 40 meters.

The relative difference of the normalized surface deflections from shallow to deep depths of all four methods may be summarized in Figure 5.9. Here the benchmark used the subsidence data above the cavity from Figure 5.3 while the other subsidences from Figures 5.4 to 5.8 were analyzed for their changes away from the shallow tunnel option. It was observed that the displacement solutions were significantly reduced of up to 88% when the depth of 40 m was chosen; only the Peck method estimate was lower at 65% but otherwise suggested a similar trend. The curve above the Peck method appeared to be lumped together but should be viewed as three distinct plots due to the closeness of the calculated error values. The large reduction of subsidences makes sense as there is more ground layers above the cavity which provide stiffness to minimize soil movement. With no soil movement at deeper excavations, the surface deflections become less pronounced.

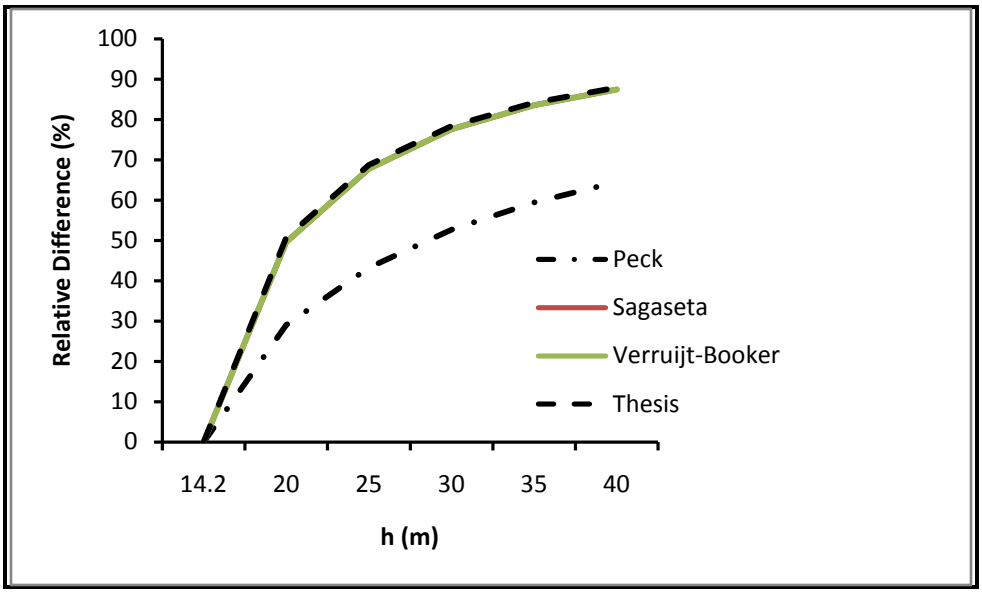

Fig.5.9 Relative difference plot for the various depths. The curve above the Peck method is composed of three other methods. The differences calculated were close to one of another to have created the appearance of having them lumped together.

5.8 Qualitative Predictions

The normalized representations as defined by Eqs. (4.2.1) and (4.2.2) are discussed in this section. When plotted, these normalized equations as shown in Figures 5.10 and 5.11 also depict a settlement trough distribution resembling the subsidence discussed above. The key distinction here was to use the ratio $\frac{x}{h}$ for a rapid estimate of potential surface settlements with the combined effects the ovalization term, depth, cavity radius and soil property as provided by Poisson's ratio.

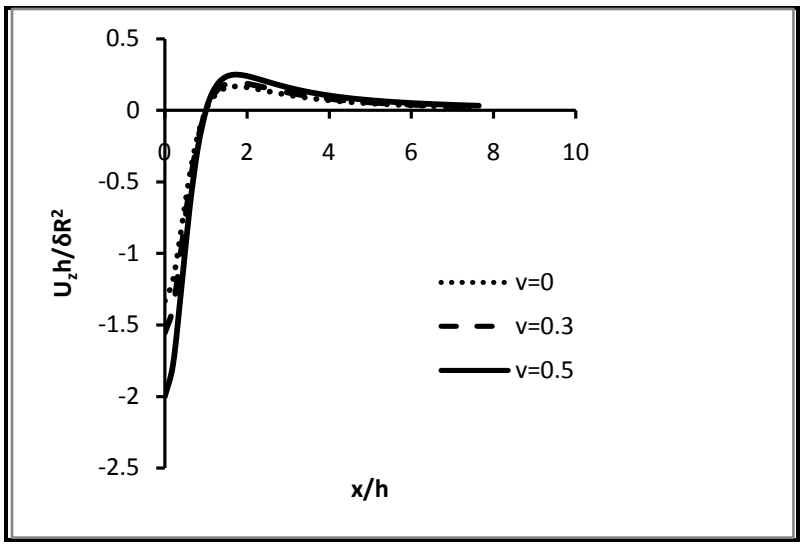

Fig.5.10 Normalized plot for the first ovalization with various Poisson's ratios.

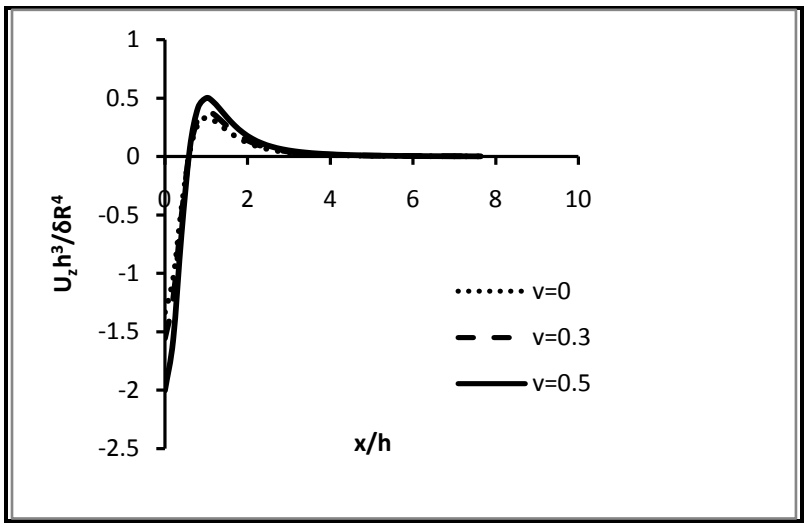

Fig.5.11 Normalized plot for the second ovalization term with various Poisson's ratios.

If the variable $\frac{x}{h}$ is arbitrarily positioned farther away from the tunnel, the influence of either $\frac{u_z h}{\delta R^2}$ or $\frac{u_z h^3}{\delta R^4}$ are diminished and eventually contribute nothing with respect to the subsidence. The reverse is true so when $\frac{x}{h}$ is measured closer to the cavity, then $\frac{u_z h}{\delta R^2}$ (or $\frac{u_z h^3}{\delta R^4}$)

begins to increase its effect on the subsidence and will peak at its maximum located at the center of the tunnel. Thus the surface settlements may be predicted to be at its highest by examining the relative value of $\frac{x}{h}$.

An additional observation could be made when various Poisson's ratios may be factored in. In this case, a range between 0 and 0.5 was examined and multiplied with both $\frac{u_z h}{\delta R^2}$ and $\frac{u_z h^3}{\delta R^4}$. When plotted, at one end where the soil is compressible (υ = 0), the distribution suggests that the subsidence tends to be lesser when compared to the incompressibility state at 0.5 by a change of 0.667 with the settlements increasing.

The quantitative significance of the heave in Figures 5.10 and 5.11 between the 1 and 2 of the horizontal axis could be examined by testing the influence of the ratio of the second over the first ovalization term and checking its impact of the tunnel radius over the depth placement. As depicted in Figure 5.12, the decrease of the ratio $\frac{h}{R}$ suggests a stronger contribution from both ovalization terms in the order of 2 to 10 times of the subsidence equation; and for the reverse, if the tunnel placement depth is deeper will then increase $\frac{h}{R}$ thereby making the need of the second ovalization negligible. Based on these observations, it could be seen that the derived general subsidence may treat the Verruijt-Booker equation as a special case depending on the placement depth.

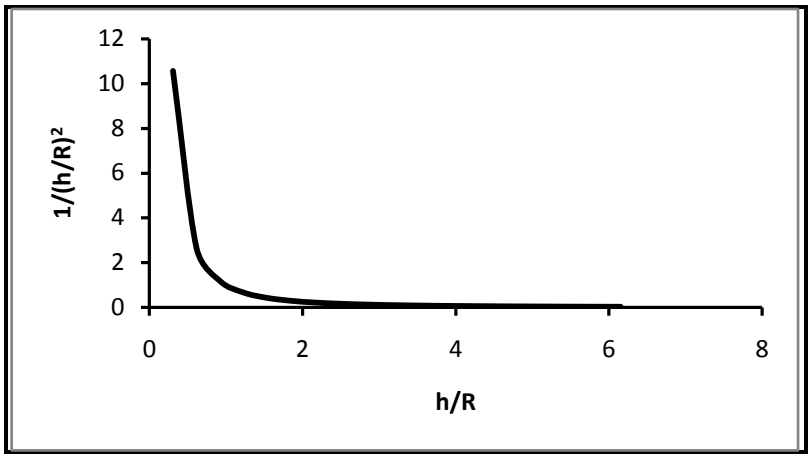

Fig.5.12 Influence of the ovalization term varied according to the placement depths of the tunnel.

In addition, the real root of Figures 5.10 and 5.11 could be determined to be equal to $\frac{x}{h}=\sqrt{-\frac{3R^2}{2h^2}+\sqrt{\frac{9R^4}{4h^4}+\frac{R^2}{h^2}+1}}$. Based on this formula, a plot distribution was constructed as shown in Figure 5.13 and indicates that if the tunnel placement for deeper depths were chosen the excessive heave tends to stabilze or level off. For the root-based plot, the vertical axis was determined by the values of the derived root solution as compared to the other nomralized graphs.

For this thesis which considered shallow tunnels, the $\frac{R}{h}$ at 0.331 indicated that the position of $\frac{x}{h}$ at 1.0 signals the presence of ground movement attempting to counterbalance a downward surface deflection above the cavity. Other $\frac{R}{h}$ values above 0.331 shows the curve decreasing and eventual levelling which corresponds to Figures 5.10 and 5.11.

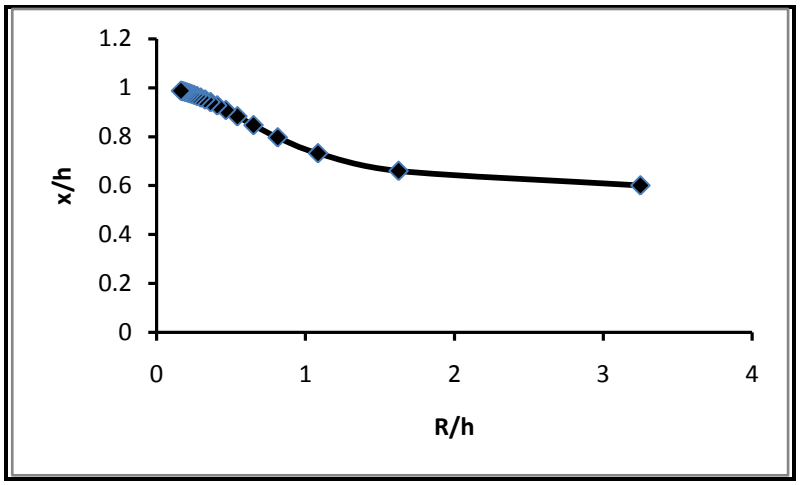

Fig.5.13 The effects of heaving may be found by examining by examining the relation of the tunnel placement depths.

Chapter 6 Conclusion

A new displacement equation linking the classical Kirsch solution and recent virtual image method of Sagaseta was derived. Essentially, the final subsidence equations used those tools to convert a half to full-space problem were only contributed from the virtual image component existing in the upper plane. The derivation incorporated higher order terms and obtained a new different pair of coefficients ε and δ for which the original VB paper does not explicitly state nor detail in steps their arrival towards the solution. Other subsidence equations were also discussed and compared to one of another using actual data from a project site.

General predictions were made with regard to a variety of depths and their respective normalized settlements above the tunnel. These predictions used a parametric-based methodology to compare the 4 displacement methods for 5 different tunneling options placed from shallow to deeper depths. It was determined that if tunneling construction chose a deeper zone for boring, the surface deflections would become less apparent. Irrespective of the subsidence methods, the quantitative conclusions were similar.

Qualitative observations were also made and directed to the thesis derived equations. The generalized VB equation was able to determine the correct direction of the tunnel deformation pattern. The amount of vertical forces exerted at the crown and base tends to move towards the center thereby pushing the lateral ends to expand horizontally. Based on this recognition of the impact of the forces that imparts deformation without significant contribution from the radial strain, simple observations can be made from the subsidence equation (4.1.105). The method required normalizing the higher-order terms for its displacement to ovalization

against the relative lateral position to the placement depth of the tunnel $\frac{x}{h}$. The normalization analysis also included a range of Poisson's ratio between 0 and 0.5 for different soil compressibility.

In closing, the entire confirmation or verification process undergone in this study if implemented for an actual tunnel construction should be repeated for certain distances representative of the subsurface terrain. These traversed segments may encounter a new soil medium requiring different soil properties such as Poisson's ratio and elastic modulus, and possibly change in tunnel depth to be catalogued, but nevertheless can adopt the methodologies described in this work to predict a viable subsidence and take action.

Appendix A- Calculation for the *P(a)* Terms

The Table 3.1 consisted of a summarized sequence of differentiation in order to evaluate the integral. In this section, all the explicit terms will be calculated to make sense of the subsequent substitution required to determine the virtual-based deflections.

The starting point is to consider the Fourier cosine transform defined below

$$\int_0^\infty \frac{\cos(ax)}{x^2+h^2}dx = F_c\left[\frac{1}{x^2+h^2}\right] = \frac{\pi\exp(-ah)}{2h} \tag{A.1}$$

and by some differentiation steps will it enable the evaluation of *P(a)*. For reference *P(a)* is restated here as $P(a) = -\int_0^\infty \sigma_{zz}\cos(ax)dx$ where σ_{zz} was derived as

$$\sigma_{zz} = -\frac{4\varepsilon R^2 G\left(h^2-x^2\right)}{\left(x^2+h^2\right)^2} - \frac{16\delta R^2 G\left(3h^2x^2-h^4\right)}{\lambda\left(x^2+h^2\right)^3} - \frac{12\delta R^4 G}{\lambda\left(x^2+h^2\right)^4}\left(-6h^2x^2+h^4+x^4\right) \tag{A.2}$$

The first term from (A.2) required the operation on both sides of (A.1) as $\frac{\partial}{\partial h}$

$$\int_0^\infty \frac{\partial}{\partial h}\left[\frac{\cos(ax)}{x^2+h^2}\right]dx = -\int_0^\infty \frac{2h\cos(ax)}{\left(x^2+h^2\right)^2}dx \tag{A.3}$$

$$\frac{\partial}{\partial h}\left[\frac{\pi\exp(-ah)}{2h}\right]=\frac{\pi\exp(-ah)}{2h}+\frac{a\pi\exp(-ah)}{2h^2}=\frac{\pi\exp(-ah)}{2h}\left(1+\frac{1}{h}\right) \tag{A.4}$$

which leads to

$$4\varepsilon R^2G\int_0^\infty\frac{h^2\cos(ax)}{\left(x^2+h^2\right)^2}dx=-\varepsilon R^2G\left[-\frac{\pi\exp(-ah)}{h}-\pi a\exp(-ah)\right] \tag{A.5}$$

The second part of the first term of (A.2) requires $\frac{\partial}{\partial h}\rightarrow\frac{\partial^2}{\partial a^2}\left(\frac{\partial}{\partial h}\right)$ and gets

$$4\varepsilon R^2G\int_0^\infty\frac{x^2\cos(ax)}{\left(x^2+h^2\right)^2}dx=\varepsilon R^2G\left[\frac{\pi\exp(-ah)}{h}-\pi a\exp(-ah)\right] \tag{A.6}$$

Subtracting (A.5) and (A.6) will verify Eq. (4.1.81).

For each derivative as was described for computing the second term of (A.2), it will be advantageous to isolate the left-side to have the form of (A.1) and simplify with the right-side differentiation. The common differentiation sequence of $\frac{\partial^2}{\partial h^2}$ obtains

$$\int_0^\infty\frac{\cos(ax)}{\left(x^2+h^2\right)^3}dx=\frac{\pi}{16}\left[\frac{3}{h^5}+\frac{3a}{h^4}+\frac{a^2}{h^3}\right]\exp(-ah) \tag{A.7}$$

The mixed-term product $3h^2x^2$ is handled by performing $\frac{\partial^2}{\partial a^2}\left(\frac{\partial^2}{\partial h^2}\right)$ and h^4 term occurring as the numerator of (A.2) is obtained by multiplying h^4 of (A.7) yielding

$$\frac{16\delta R^2 G}{\lambda}\int_0^\infty \frac{3h^2x^2\cos(ax)}{\left(x^2+h^2\right)^3}dx = \frac{\delta R^2 G\pi}{\lambda}\left(3a^2h+3a+\frac{3}{h}\right)\exp(-ah) \tag{A.8}$$

$$\frac{16\delta R^2 G}{\lambda}\int_0^\infty \frac{h^4\cos(ax)}{\left(x^2+h^2\right)^3}dx = \frac{\delta R^2 G\pi}{\lambda}\left(\frac{3}{h}+3a+a^2h\right)\exp(-ah) \tag{A.9}$$

If (A.8) and (A.9) are subtracted, Eq. (4.1.82) will be established.

In evaluating the remaining component of (A.2), it will be recognized beforehand that there is a common differentiation sequence with respect to *h* three times consecutively. Thus, after the third differentiation $\frac{\partial^3}{\partial h^3}$, the result should have the form

$$\int_0^\infty \frac{\cos(ax)}{\left(x^2+h^2\right)^4}dx = \frac{\pi}{96}\left(\frac{15}{h^7}+\frac{15a}{h^6}+\frac{6a^2}{h^5}+\frac{a^3}{h^4}\right)\exp(-ah) \tag{A.10}$$

The step towards obtaining for the numerator containing the mixed-term $6h^2x^2$ and x^4 products are to differentiate (A.10) with respect to *a* twice and four-times respectively. In doing so, these relations will be established

$$\frac{12\delta R^4 G}{\lambda}\int_0^\infty \frac{6h^2x^2\cos(ax)}{\left(x^2+h^2\right)^4}dx = -\frac{\delta R^4 G\pi}{\lambda}\left(\frac{9}{4h^3}+\frac{9a}{4h^2}-\frac{3a^3}{4}\right)\exp(-ah) \tag{A.11}$$

$$\frac{12\delta R^4 G}{\lambda}\int_0^\infty \frac{h^4\cos(ax)}{\left(x^2+h^2\right)^4}dx = -\frac{\delta R^4 G\pi}{\lambda}\left(\frac{15}{8h^3}+\frac{15a}{8h^2}+\frac{3a^2}{4h}+\frac{a^3}{8}\right)\exp(-ah) \tag{A.12}$$

$$\frac{12\delta R^4 G}{\lambda}\int_0^\infty \frac{x^4\cos(ax)}{\left(x^2+h^2\right)^4}dx = -\frac{\delta R^4 G\pi}{\lambda}\left(-\frac{3}{8h^3}-\frac{3a}{8h^2}+\frac{3a^2}{4h}+\frac{a^3}{8}\right)\exp(-ah) \tag{A.13}$$

By adding (A.11) through (A.13) will confirm Eq. (4.1.83).

Appendix B- Fourier Sine and Cosine Transforms

In this section, the Fourier sine $F_s[a]$ and cosine $F_c[a]$ transforms used in establishing the supplemental distance relations required for the virtual deflection equations development will be expanded. In the following derivations, it will be taken for granted that the relevant transforms are valid from any reputable mathematical hand tables.

The relevant definition for the Fourier sine $F_s[a]$ and cosine $F_c[a]$ transforms was taken as the asymmetric representations

$$F_s[a] = F_s\left[f(a)\right] = \int_0^\infty f(a)\sin(ax)da \tag{B.1}$$

$$F_c[a] = F_c\left[f(a)\right] = \int_0^\infty f(a)\cos(ax)da \tag{B.2}$$

It will be noted that in the process of substituting *P(a)* into Eqs. (4.88) or (4.89), the exponential part may be merged and in the context of (B.1) and (B.2) can the following definitions be seen

$$\int_0^\infty \exp\left[-a(h+z)\right]\sin(ax)\,da \tag{B.3}$$

$$\int_0^\infty \exp\left[-a(h+z)\right]\cos(ax)\,da \tag{B.4}$$

For simplicity, (B.4) will be considered but the derivation details are similar for (B.3). From (4.63), the following distance relations for the upper plane were used

$$\left.\begin{aligned} z_2 &= h + z \\ r_2^2 &= x^2 + z_2^2 \end{aligned}\right\} \tag{B.5}$$

and when substituted into (B.4) the integral becomes

$$\int_0^\infty \exp\left(-az_2\right)\cos\left(ax\right)da \tag{B.6}$$

Also in the substitution of *P(a)* into the displacement integrals of Sneddon [26], the constant a^b will often appear. From the cosine transform definitions of (4.1.87) and (4.1.88), their representations are repeated here as

$$F_c\left[\exp\left(-az\right)\right] = \frac{z}{x^2 + z^2} \tag{B.7}$$

$$F_c\left[a^{b-1}\exp\left(-az\right)\right] = \frac{\Gamma\left(b\right)\cos\left(b\arctan\dfrac{x}{z}\right)}{\left(x^2 + z^2\right)^{b/2}} \tag{B.8}$$

The particular cases to be examined are with b = 2, 3 and 4. When b = 1, (B.8) is reduced to (B.7).

For b = 2, (B.8) will take the form as

$$F_c\left[a\exp\left(-az_2\right)\right]=\frac{\Gamma\left(2\right)\cos\left[2\arctan\left(\frac{x}{z_2}\right)\right]}{\left(x^2+z_2^2\right)} \tag{B.9}$$

where $\Gamma\left(r+1\right)=r!$ is the gamma or factorial function. Letting $\theta=\arctan\left(\frac{x}{z_2}\right)$, then $\tan\theta=\frac{x}{z_2}$ from which $\cos\theta=\frac{z_2}{\sqrt{x^2+z_2^2}}=\frac{z_2}{r_2}$. Also, $\cos 2\theta=2\cos^2\theta-1$ must be used or in its equivalent analytic form $\cos 2\theta=\frac{2z_2^2-r_2^2}{r_2^2}=\frac{2z_2^2-x^2-z_2^2}{\left(x^2+z_2^2\right)^2}$. Thus, (B.9) now becomes

$$F_c\left[a\exp\left(-az_2\right)\right]=-\frac{\left(x^2-z_2^2\right)}{\left(x^2+z_2^2\right)^2}=-\frac{\left(x^2-z_2^2\right)}{r_2^4} \tag{B.10}$$

which was the identity stated for (4.1.94).

For b = 3, (B.8) will take the form as

$$F_c\left[a^2\exp\left(-az_2\right)\right]=\frac{2\cos\left[3\arctan\left(\frac{x}{z_2}\right)\right]}{\left(x^2+z_2^2\right)^{3/2}} \tag{B.11}$$

Here Γ(3) = 2, and the identity $\cos 3\theta = 4\cos^3\theta - 3\cos\theta$ was used. In a similar analytic manner from above and substitutions made gets

$$F_c\left[a^2\exp\left(-az_2\right)\right] = -\frac{2z_2\left(3x^2 - z_2^2\right)}{\left(x^2 + z_2^2\right)^3} = -\frac{2z_2\left(3x^2 - z_2^2\right)}{r_2^6} \tag{B.12}$$

thereby established identity (4.1.95).

Finally, setting $b = 4$, Γ(4) = 6 along with $\cos 4\theta = 8\cos^4\theta - 8\cos^2\theta + 1$ was referred to, making (B.8)

$$F_c\left[a^3\exp\left(-az_2\right)\right] = \frac{6\cos\left[4\arctan\left(\frac{x}{z_2}\right)\right]}{\left(x^2 + z_2^2\right)^{4/2}} \tag{B.13}$$

Repeating the same analytic form and substituting into $\cos 4\theta$ gets $\frac{1}{r_2^4}\left(\frac{48z_2^4}{r_2^4} - \frac{48z_2^2}{r_2^2} + 6\right)$. Thus,

$$F_c\left[a^3\exp\left(-az_2\right)\right] = \frac{6}{r_2^4} - \frac{48z_2^2}{r_2^6} + \frac{48z_2^4}{r_2^8} \tag{B.14}$$

and verifies identity (4.1.96).

References

1. **Ameen, M.** *Computational Elasticity- Revised Edition.* Oxford, U.K. : Alpha Science International Ltd., 2008.

2. **Bobet, A.** Analytical Solutions for Shallow Tunnels in Saturated Ground. *ASCE J. of Engineering Mechanics.* December 2001, Vol. 127, 12, pp. 1258-1266.

3. **Clough, G. W. and Schmidt, B.** Design and Performance of Excavatiion and Tunnels in soft clay. *Soft Clay Engineering.* Amsterdam : Elsevier, 1981, pp. 569-634.

4. **Craig, R. F.** *Craig's Soil Mechanics, 7th ed.* London, U.K. : Spon Press- Taylor and Francis Group, 2004.

5. **Gonzalez, C. and Sagaseta, C.** Patterns of Soil Deformations Around Tunnels-Application to the Extension of Madrid metro. *Computers and Geotechnics.* January 2001, Vol. 28, pp. 445-468.

6. **Holtz, R. D. and Kovacs, W. D.** *An Introduction to Geotechnical Engineering.* Upper Saddle River, NJ : Prentice-Hall Inc. , 1981.

7. **Hughes, W. F. and Brighton, J. A.** *Schaum's Outline of Fluid Dynamics, 2nd ed.* New York : McGraw-Hill, 1991.

8. *The Excavation of a Shallow Tunnel Below a Commercial Center.* **Jordan, M. F. and Ramos, E. del M. et. al.** Toulouse, France : ISSMGE, Technical Committee TC28:, 2002. Geotechnical Aspects of Underground Construction in Soft Ground. pp. 47-52.

9. **Kolymbas, D.** *Tunneling and Tunneling Mechanics.* Berlin, Germ. : Springer, 2005.

10. **Kooi, C. B. and Verruijt, A.** Interaction of Circular Holes in an Infinite Elastic Medium. *Tunneling and Underground Space Technology.* January 2001, Vol. 16, 1, pp. 59-62.

11. **Leca, E. and New, B.** ITA/AITES Report 2006 on Settlements Induced by Tunneling in Soft Ground. *Tunneling and Underground Space Technology.* February 2007, Vol. 22, pp. 119-149.

12. *Soil Movements Around a Tunnel in Soft Soils.* **Lee, C. J., Wu, B. R. and Chiou, S. Y.** s.l. : National Science Council, Taipei, TAIWAN, 1999. Proceedings of the National Science Council, Republic of China. Part A, Physical science and engineering. Vol. 23(2), pp. 235-247.

13. **Lee, K. M, Rowe, R. K. and Lo, K. Y.** Subsidence Owing to Tunneling I-Estimating the Gap Parameter . *Can. Geotech. J.* 1992, Vol. 29, pp. 929-940.

14. *Predicting Settlement Due to Tunnelling in Clays, in Proceedings of Two Sessions at Geotech1984.* **Lo, K. Y., Ng, M. C. and Rowe, R. K.** New York, NY : ASCE-Geotechnical Engineering Division, 1984.

15. **Loganathan, N. and Poulos, H. G.** Analytical Prediction for Tunneling-Induced Ground Movements in Clays. *ASCE J. Geotechnical and Geoenvironmental Engineering.* September 1998, Vol. 124, 9, pp. 846-856.

16. **Mahtab, M. A. and Grasso, P.** *Geomechanics Principles in the Design of Tunnels and Caverns in Rocks.* Amsterdam, the Netherlands : Elsevier Science Publishers, 1992.

17. **Melis, M., Medina, L. and Rodriguez, J. M.** Prediction and Analysis of Subsidence Induced by Shield Tunneling in the Madrid Metro Extension. *Can., Geotech J.* 2002, Vol. 39, pp. 1273-1287.

18. **Migliazza, M., Chiorboli, M. and Giani, G. P.** Comparison of Analytical Method-3D Finite Element Model with Experimental Subsidence Measurements Resulting from Extension of the Milan Underground. *Computers and Geotechnics.* 2009, Vol. 36, pp. 113-124.

19. **Osman, A. S., Bolton, M. D. and Mair, R. J.** Predicting 2D Ground Movements Around Tunnels in Undrained Clay. *Geotechnique.* September 2006, Vol. 56, 9, pp. 597-604.

20. **Park, K. H.** Analytical Solution for Tunneling-induced Ground Movement in Clays. *Tunneling and Underground Space Technology.* May 2005, Vol. 20, 3, pp. 249-261.

21. —. Elastic Solution for Tunneling-Induced Ground Movements in Clays. *ASCE International Journal of Geomechanics.* December 2004, Vol. 4, 4, pp. 310-318.

22. *Deep Excavtion and Tunneling in Soft Ground.* **Peck, R. B.** Mexico : s.n., 1969. Proceedings of the 14th International Conference on Soil Mechanics and Foundation Engineering. Vol. 4 (State of the Art), pp. 225-290.

23. **Sagaseta, C.** Analysis of Undrained Soil Deformation Due to Ground Loss. *Geotechnique.* 1987, Vol. 37, 3, pp. 301-320.

24. **Savage, W. Z.** Prediction of Vertical Displacements in a Subsiding Elastic Layer. *U. S. Geological Survey -Geophysical Review Letters.* March 1981, Vol. 8, 3, pp. 195-198.

25. **Scechy, K.** *The Art of Tunneling.* Budapest, Hungary : Akademiai Kiado, 1973.

26. **Sneddon, I. N.** *Fourier Transforms.* New York : McGraw-Hill, 1951.

27. **Spiegel, M. R.** *Schaum's Outline - Mathematical Handbook of Formulas and Tables.* New York : McGraw-Hill, 1968.

28. **Timoshenko, S. and Goodier, J. N.** *Theory of Elasticity, 2nd ed.* Toronto : McGraw-Hill Book Company, 1951.

29. **Verruijt, A. and Booker, J. R.** Surface Settlement Due to Deformation of a Tunnel in an Elastic Half Plane. *Geotechnique.* 1996, Vol. 46, 4, pp. 753-756.

30. **Wahlstrom, E. E.** *Tunneling in Rock.* Amsterdam, the Netherlands : Elsevier Scientific Publishing, 1973.

31. **Yu, H.** *Cavity Expansion Methods in Geomechanics.* London : Kluwer Academic Publishers, 2000.